(4)

Annual Letter Report

Growth, Characterization and Device Development in Monocrystalline Diamond Films

Supported by the Innovative Science and Technology Office
Strategic Defense Initiative Organization
Office of Naval Research
under Contract #N00014-90-J-1604
for the period January 1, 1992–December 31, 1992

R. F. Davis, J. T. Glass, R. J. Nemanich* and R. J. Trew**
K. S. Ailey-Trent, L. Bergman*, T. P. Humphreys*, D. Kester, K. L. More,
B. R. Stoner, K. F. Turner*, J. van der Weide*, and S. D. Wolter
North Carolina State University
c/o Materials Science and Engineering Department
*Department of Physics
**Electrical and Computer Engineering
Raleigh, NC 27695

December 31, 1992

REPORT DOCUMENTATION PAGE

Form Approved
OMB No 0704-0188

1. AGENCY USE ONLY (Leave blank)	2. REPORT DATE	3. REPORT TYPE AND DATES COVERED
	December, 1992	Annual Letter 1/1/92–12/31/92

4. TITLE AND SUBTITLE

Growth, Characterization and Device Development in Monocrystalline Diamond Films

5. FUNDING NUMBERS

s400003srr08
1114SS
N00179
N66005
4B855

6. AUTHOR(S)

Robert F. Davis

7. PERFORMING ORGANIZATION NAME(S) AND ADDRESS(ES)

North Carolina State University
Hillsborough Street
Raleigh, NC 27695

8. PERFORMING ORGANIZATION REPORT NUMBER

N00014-90-J-1604

9. SPONSORING / MONITORING AGENCY NAME(S) AND ADDRESS(ES)

Department of the Navy
Office of the Chief of Naval Research
800 North Quincy Street, Code 1513:CMB
Arlington, VA 22217-5000

10. SPONSORING / MONITORING AGENCY REPORT NUMBER

11. SUPPLEMENTARY NOTES

12a. DISTRIBUTION / AVAILABILITY STATEMENT

Approved for Public Release—Distribution Unlimited

12b. DISTRIBUTION CODE

13. ABSTRACT (Maximum 200 words)

Investigations concerned with bias-enhanced nucleation (BEN) of diamond films revealed that the substrate holder must be diamond coated to achieve this phenomenon. This suggests that some unique property of diamond is responsible for the increased nucleation densities. The carbide-forming substrates tended to nucleate more rapidly than other substrates, thus indicating that the carbide forming nature of the substrate may play an important role. A statistical experimental design was implemented to optimize the process parameters associated with BEN. Continued efforts regarding the surface and interface properties of diamond showed an increased density of impurity-related defects during the initial stages of growth. Angle resolved photo-emission has revealed a negative electron affinity (NEA) on diamond(111) after cleaning and after sub-monolayer deposition of Ti. The Schottky barrier height of Ti on diamond has also been measured. A model is proposed for the observed NEA. The device modeling research on MESFETs was expanded to include MOSFETs and JFETs. The NCSU large-signal FET model was augmented with simulations using Stanford's Pisces IIB simulator. An interface program has been written to couple the NCSU and Stanford models and used to investigate the dc performance of three diamond FETs. Good agreement between measured and simulated data was obtained. In related research, films of cubic(c)-BN were deposited on Si(100) and diamond (100) substrates using ion beam assisted deposition. The results were investigated by FTIR and HRTEM. Analysis of the films indicates that compressive stresses produced by ion bombardment and the interstitial incorporation of Ar result in compressive stresses which may be the cause the formation of the c-BN.

14. SUBJECT TERMS	15. NUMBER OF PAGES
diamond thin films, bias-enhanced nucleation, impurity-related defects, negative electron affinity, Schottky barrier height, Titanium contacts, device modeling, MESFET, MOSFET, JFET, cubic-BN, FTIR	61
	16. PRICE CODE

17. SECURITY CLASSIFICATION OF REPORT	18. SECURITY CLASSIFICATION OF THIS PAGE	19. SECURITY CLASSIFICATION OF ABSTRACT	20. LIMITATION OF ABSTRACT
UNCLAS	UNCLAS	UNCLAS	SAR

Table of Contents

I.	Introduction	1
II.	Process Parameter and Substrate Effect of Bias-enhanced Nucleation	3
III.	Properties of Interfaces of Diamond	7
IV.	Modeling of Microwave MESFET Electronic Devices Fabricated from Semiconducting Diamond Thin Films	30
V.	Cubic Boron Nitride Thin Film Growth	37
VI.	Phase Evolution in Boron Nitride Thin Films	50
VII.	Distribution List	60

I. Introduction

Diamond as a semiconductor in high-frequency, high-power transistors has unique advantages and disadvantages. Two advantages of diamond over other semiconductors used for these devices are its high thermal conductivity and high electric-field breakdown. The high thermal conductivity allows for higher power dissipation over similar devices made in Si or GaAs, and the higher electric field breakdown makes possible the production of substantially higher power, higher frequency devices than can be made with other commonly used semiconductors.

In general, the use of bulk crystals severely limits the potential semiconductor applications of diamond. Among several problems typical for this approach are the difficulty of doping the bulk crystals, device integration problems, high cost and low area of such substrates. In principal, these problems can be alleviated via the availability of chemically vapor deposited (CVD) diamond films. Recent studies have shown that CVD diamond films have thermally activated conductivity with activation energies similar to crystalline diamonds with comparable doping levels. Acceptor doping via the gas phase is also possible during activated CVD growth by the addition of diborane to the primary gas stream.

The recently developed activated CVD methods have made feasible the growth of polycrystalline diamond thin films on many non-diamond substrates and the growth of single crystal thin films on diamond substrates. More specifically, single crystal epitaxial films have been grown on the {100} faces of natural and high pressure/high temperature synthetic crystals. Crystallographic perfection of these homoepitaxial films is comparable to that of natural diamond crystals. However, routes to the achievement of rapid nucleation on foreign substrates and heteroepitaxy on one or more of these substrates has proven more difficult to achieve. This area of study has been a principal focus of the research of this contract.

At present, the feasibility of diamond electronics has been demonstrated with several simple experimental devices, while the development of a true diamond-based semiconductor materials technology has several barriers which a host of investigators are struggling to surmount. It is in this latter regime of investigation that the research described in this report has and continues to address.

Boron nitride is similar to carbon in having three crystalline structures: a layered hexagonal structure (*h*-BN) corresponding to graphite, the cubic structure (*c*-BN) analogous to diamond, and a rare hexagonal wurtzite structure (*w*-BN) corresponding to Lonsdaleite. The last two phases are metastable under normal environmental conditions. An amorphous phase (*a*-BN) is also common in films and coatings.

The extreme mechanical and thermal properties of *c*-BN make it useful for wear-resistant tools for the machining of steels, for corrosion resistant and electrically insulating parts, and for heat sinks for electronic devices. It has also recently been shown that bulk single crystals of

this wide bandgap (E_g≈6.4 eV) semiconductor can be doped with both n- and p-type impurities and that light emitting p-n junctions can be produced. This phase combined with other BN phases, has also been achieved in thin film form via physical vapor deposition and chemical vapor deposition methods.

Most researchers growing BN films use FTIR spectroscopy for phase identification. The cubic phase of BN has a distinct absorption peak at about 1080 cm^{-1}. The hexagonal, turbostratic (disordered hexagonal), and amorphous phases have primary and secondary absorption peaks at 1370 and 780 cm^{-1}, respectively. Thus, these non-cubic phases cannot be distinguished using FTIR. A commonly reported feature of these spectra obtained from analyses of the total thickness of the films wherein the presence of *c*-BN is apparent is the indication of various amounts of the hexagonal and/or amorphous phases. However, the actual evolution of these phases must be determined by HRTEM.

In this reporting period, some of the important parameters which positively influence the bias-enhanced, oriented nucleation of diamond have been investigated. Additional diamond nucleation studies have been conducted using scanning tunneling microscopy. The negative electron affinity has also been probed with and without Ti deposits. The ongoing modeling studies for high frequency devices in diamond has been broadened to include MOSFETs and JFETs as well as mono- and polycrystalline materials. Finally, a significant effort concerned with the kinetics, mechanisms and phase evolution of BN phases deposited using ion beam-assisted electron beam evaporation on Si(100) and diamond (100) has been conducted.

The following subsections detail the experimental procedures for each of the aforementioned studies, discuss the results and provide conclusions and references for these studies. Note that each major section is self-contained with its own figures, tables and references.

II. Process Parameter and Substrate Effect of Bias-enhanced Nucleation

A. Introduction

Bias-enhanced nucleation (BEN) via microwave plasma chemical vapor deposition (MPCVD) was utilized to investigate the influence of this process on various substrate materials. In addition, a statistical experimental design (SED) has been implemented to optimize the process parameters associated with BEN. Negatively biasing the substrate as an in-situ pretreatment has been attributed to greatly enhancing the nucleation density of diamond on silicon [1] and has also been utilized to epitaxially nucleate diamond on β-SiC [2].

B. Results and Discussion

The initial findings of this study revealed that it was essential that the substrate holder be diamond coated while performing BEN as shown in Figure 1. It was discovered that the uncoated molybdenum substrate holder resulted in little or no observable diamond nucleation during the biasing process. To determine the importance of the diamond coating, both alumina and graphite substrate holder coatings were tested. Neither were successful in enhancing the diamond nucleation via biasing, suggesting that some unique property of diamond is responsible for the increased nucleation densities. There does appear to be a critical amount of diamond on the substrate holder that is essential for reproducible results. This is shown in Figure 2 which indicates that as more diamond is coated on the substrate holder the biasing time for the formation of a continuous film becomes constant. Also of interest in this plot is the observation of an increase in current with diamond coating thickness. Furthermore, it was found that when other materials surrounded the substrate, including metals, the bias current decreased by up to 80%. This suggests that the diamond is acting as an electron emission source.

After obtaining a greater understanding of the BEN process various substrates were chosen for study based on their affinity for carbon. In a previous work it was observed that silicon was much more influenced by the negative substrate bias than was copper [3]. This reveals that the carbide forming nature of silicon compared to the non-carbide forming nature of copper may give an indication of the class (i.e. carbide or non-carbide forming) of substrate material which may yield the optimum results. For this reason the carbide forming refractory elements, Ti, Nb, W, and Ta, were chosen to study in greater detail. In Figure 3 a plot of the nucleation density versus bias time is shown for the different refractory elements in addition to silicon, copper, and germanium. This plot indicates that, among the various carbide forming substrates, silicon shows a dramatically higher nucleation efficiency. All the refractory elements tended to nucleate more rapidly than the non-carbide forming germanium and copper substrates thus strongly suggesting that the carbide forming nature of the substrate may play an

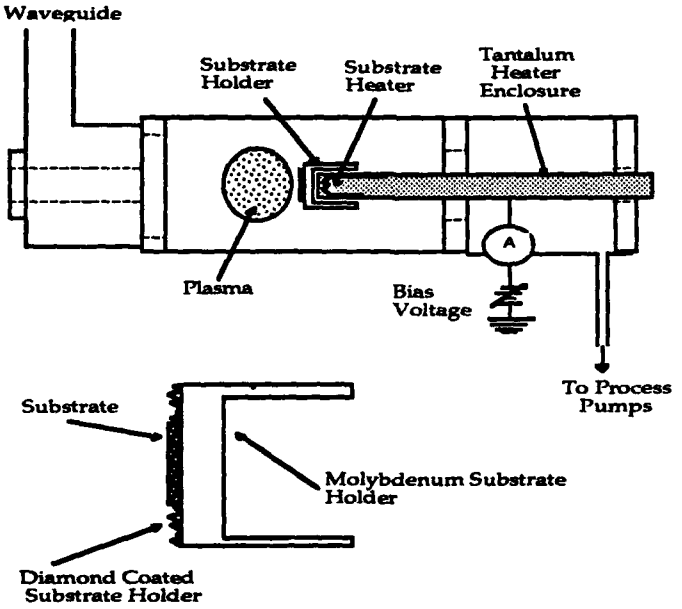

Figure 1. Microwave Plasma Chemical Vapor Deposition chamber and diamond coated substrate holder.

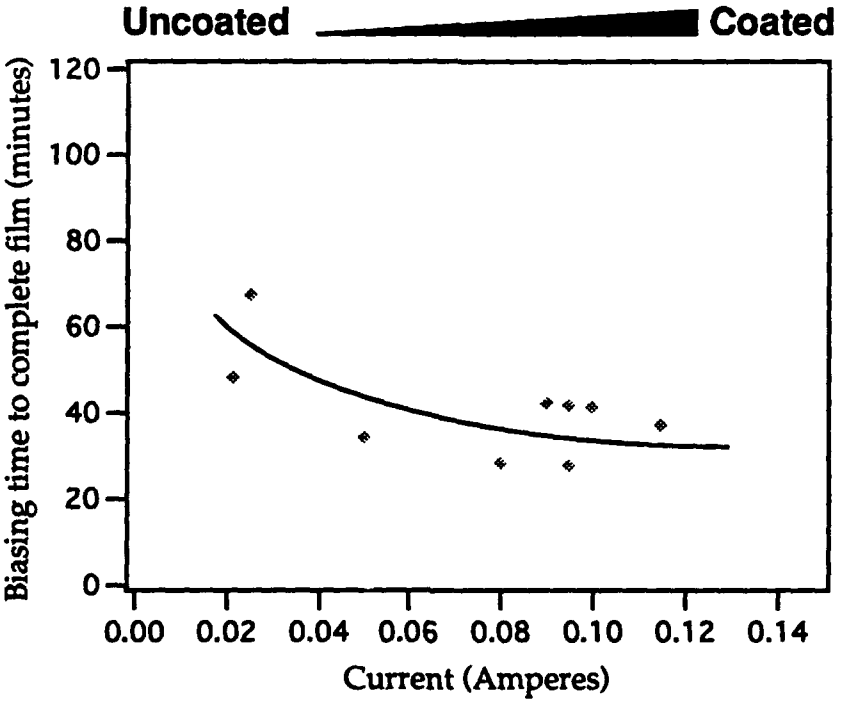

Figure 2. Time for the formation of a continuous diamond film versus the amount of coated substrate diamond.

important role in the BEN process. Several possible explanations were considered for the trends established between the various substrate materials. These being the carbon diffusivity, the heat of formation of the carbide, and the heat of sublimation. Joffreau et al. [4] proposed a relationship between the nucleation kinetics and the diffusivity values of the refractory elements. There was an indication in this experimentation that the nucleation kinetics were consistent with the diffusivity values of the refractory carbides. However, there is still no conclusive evidence that relates this material property as well as the other suggested material properties to the trends established in Figure 3.

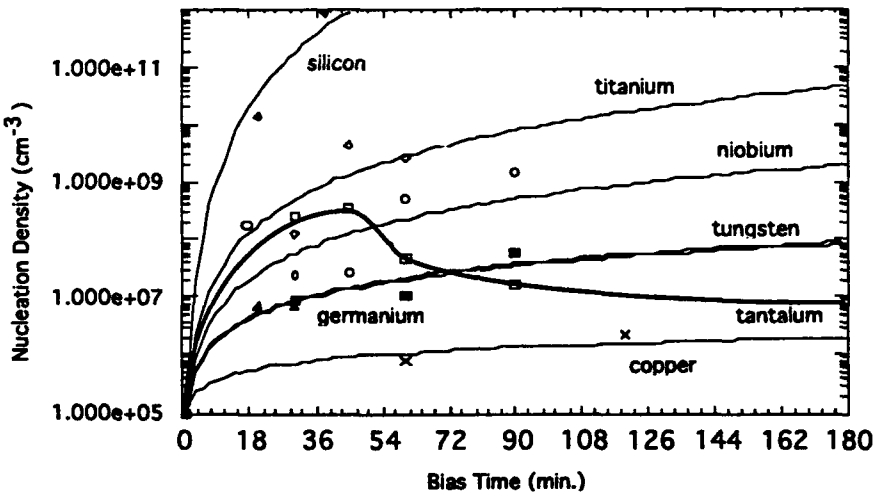

Figure 3. Nucleation density versus bias time for the refractory elements in relation to silicon and the non-carbide forming copper and germanium substrates.

The process parameters associated with BEN were studied to optimize the conditions under which this process was performed utilizing the SED. These process parameters being the substrate bias voltage, pressure, and methane concentration. In this respect, the parametric space may be isolated deriving the highest nucleation density, best film uniformity, highest diamond particle quality, and lowest bias time required for the formation of a diamond film. In addition to optimizing the parametric space of BEN these responses may also offer an insight into a better understanding of BEN in general. It was observed that under a high bias voltage and/or low pressure regime the diamond was noted to have etched from the substrate holder. In addition, no diamond was observed to have nucleated on the silicon substrates under these same conditions. Likewise, at lower bias voltages and/or higher pressures the bias current was observed to be reduced and much longer bias times were required to nucleate diamond.

C. Conclusion

In summary, a better general understanding of BEN was obtained. The SED was implemented to observe the relative influence of the process parameters for obtaining the optimum diamond films on silicon substrates. In addition, this study has explored the possibility of utilizing BEN on substrate materials other than silicon; these being the refractory elements. Silicon was observed to obtain the highest nucleation densities with respect to bias time, followed by the refractory substrates and finally the non-carbide forming germanium and copper substrates.

D. Acknowledgment

The authors wish to thank M. Veil for her assistance during experimentation. The financial support of this research was provided in part by SDIO/IST through ONR and the Kobe Steel, Ltd. Professorship at NCSU.

E. References

1. B. R. Stoner, G.-H. M. Ma, S. D. Wolter and J. T. Glass, Phys. Rev. B, **45**, 11067 (1992).
2. W. Zhu, B. R. Stoner, G.-H. M. Ma, H. S. Kong, M. W. H. Brawn and J. T. Glass, Phys. Rev. B15, (1992) (submitted).
3. S. D. Wolter, B. R. Stoner, G.-H. M. Ma and J. T. Glass, in Materials Research Society Symposium Proceedings, (in press), MRS, San Fransisco, Ca, Vol. 270.
4. P. O. Joffreau, R. Haubner, and B. Lux, Int. J. Refract. Hard Met. December, 186 (1988).

III. Properties of Interfaces of Diamond*

R.J. Nemanich, L. Bergman, K.F. Turner, J. van der Weide, and T.P. Humphreys
Department of Physics and Department of Materials Science and Engineering
North Carolina State University
Raleigh, NC 27695-8202

Results related to two different interface aspects involving diamond are described; (1) the initial stages of CVD diamond film growth, and (2) the negative electron affinity and formation of metal-diamond interfaces. The surface and interface properties are probed with STM, Raman scattering/photoluminescence and angle-resolved uv-photoemission spectroscopy (ARUPS). STM measurements of diamond nuclei on Si after various plasma growth processes show both flat and hillocked structures characteristic of 2-dimensional and 3-dimensional growth modes, respectively. STS measurements show distinct I-V characteristics of the nuclei and the substrate. The presence of optical defects and the diamond quality are studied with micro-Raman/photoluminescence measurements. The results indicate an increased density of impurity related defects during the initial stages of growth. The interface properties of Ti on natural crystal (111) and (100) surfaces are studied with ARUPS using 21.2eV HeI emission. Prior to deposition the diamond (111) is chemically cleaned, and a sharp (0.5eV FWHM) peak is observed at the position of the conduction band minimum, indicating a negative electron affinity surface. After a subsequent argon plasma clean this peak disappears, while the spectrum shows a shift of 0.5 eV towards higher energies. Upon sub-monolayer titanium deposition on (111) diamond, the negative electron affinity peak reappears. Further titanium depositions causes this titanium induced negative electron affinity peak to be attenuated, indicating that the emission originates from the interface. A similar experiment, done on the diamond (100) surface, however, does not result in a negative electron affinity. By determining the relative positions of the diamond valence band edge and the titanium Fermi level, the Schottky barrier height of titanium on diamond is measured. A model, based on the Schottky barrier height of titanium on diamond, and the work function of titanium, is proposed, for the observed titanium induced negative electron affinity.

*To appear in the Proceedings of the 7th Trieste Semiconductor Symposium on Wide-Band-Gap Semiconductors, edited by C. G. Van de Walle.

I Introduction

Continuing advances in the CVD growth of doped diamond thin films offer the possibility of diamond semiconductor devices.[1] Because large diamond substrates are, at this time, prohibitively expensive, most potential electronic applications have focussed on heteroepitaxial structures. The nucleation of diamond on non-diamond substrates has, however, proved difficult. Because of the potential for electronic applications, much effort has been focussed on the nucleation and growth of diamond on Si. While small regions of heteroepitaxial growth have recently been reported on SiC and BN substrates,[2,3] only polycrystalline growth has been achieved on Si and other commonly used substrates. In fact, without special processing of the substrate, the initial nucleation rate is so low, that no diamond growth is achieved within an exposure to the growth conditions for over 60 min. In this study, the initial growth nucleation and growth modes of diamond on Si are studied by STM and Raman photoluminescence measurements.

To achieve diamond devices, metal contacts and Schottky barriers will be critical. One of the most important advances with regards to device applications is the growth of p-type diamond with boron incorporation. This is achieved either by implantation or by incorporation during the growth. Device structures have been demonstrated with the p-type material, and it is apparent that understanding contacts and Schottky barrier properties will be critical. Because of the large band-gap, diamond has the potential of high temperature operation, thus it is critical to obtain contacts and Schottky barrier structures that are both chemically and electrically stable at high temperature operation.

A particularly interesting property of diamond is that under some surface preparation conditions, a negative electron affinity can be achieved. The term negative electron affinity means that the conduction band of the semiconductor at or near the surface is above the vacuum level (i.e.. the zero kinetic energy of an electron in free space.) In this condition electrons in the conduction band will not be bound in the sample and electron emission can occur. In this study we demonstrate that the electron affinity is dependent on the sample surface preparation. Both surface termination and overlayer coverage can substantially affect the electron affinity.

II. Experimental

The diamond films were prepared by microwave plasma CVD on 1 inch diameter n-type Si(111) or Si(100) substrates. The substrates were polished with 0.25 μm diamond powder, followed by an ultrasonic clean in TCE, acetone, methanol, a rinse with de-ionized water and then a drying with nitrogen. A 30 minute hydrogen plasma etch was performed before growth. The growth occurred at a pressure of 25 Torr, a methane to hydrogen ration of 1% with a total flow rate of 1000 sccm and a substrate temperature of ~750°C. No intentional dopant was used in the growth process. SEM micrographs were obtained of the surfaces to

show the surface topography on a large scale and to provide an estimate of the nucleation density and the evolution of growth on the surface. Raman spectroscopy and photoluminescence analysis were also performed. The subsequent growth was observed by stopping the growth process after 1.5, 3, 5, 7, 10, 17 and 40 hours of deposition.

The STM analysis of the diamond was done over a wide range of parameters. All of the analysis was performed using an Park Scientific Instruments SU-200 scanning tunneling microscope operated in the ambient atmosphere. The surfaces were scanned over several scan ranges (20Å - 5μm), tunneling currents (0.5 nA - 4.0 nA), and at both positive and negative bias voltages. With the STM used, a positive bias voltage corresponds to a voltage applied to the tip that is positive relative to the sample.

Current-voltage measurements were also performed using the STM, in a process that is called tunneling spectroscopy. In these measurements, the bias voltage is ramped from positive to negative values, and the current monitored. All current-voltage measurements presented are averaged over many voltage cycles and were representative of the I-V characteristics of the entire surface. Measurements also allowed for measurement of the surface density of states, which is proportional to the ratio of the differential conductance to the conductance.

The photoemission data presented in this paper, were obtained from natural single crystal diamond. The diamond substrates used in this study were 3 x 3 x 0.5 mm^3, type IIb wafers, with a (111) or a (100) surface orientation. These wafers are p-type semiconducting, with typical resistivities ranging from 1.3 kΩ-cm to 16 kΩ-cm. The substrates were polished with 0.25 μm diamond grit and cleaned in a boiling chromic acid solution before loading. Once in vacuum the diamond (111) was further cleaned in a plasma cleaning chamber by exposing it to a remote, RF induced, argon plasma. During the exposure the diamond was heated to 350°C. The diamond (100) was cleaned by heating it in UHV to about 600°C for 10 min. Titanium was evaporated by resistively heating a titanium filament, and spectra were taken at increasing thicknesses. The thickness of the deposited films was monitored with a crystal rate monitor. The plasma cleaning chamber is connected to the ARUPS chamber through an UHV transfer system. The photoemission was excited with 21.21 eV HeI radiation, and the data presented here was obtained with an angle resolved ultraviolet photoemission spectroscopy (ARUPS) system, which included a 50 mm radius hemispherical analyzer with an angular resolution of 2°. A bias voltage of ~1 V or less, was applied to the sample during the measurements to overcome the work function of the analyzer. The bias voltage allowed the collection of the low energy electrons, which show the negative electron affinity effect.

III. Results and Discussion

A. Nucleation and Initial Growth

The results of the investigation of the initial stages of diamond growth can be broken down into different properties: changes in the surface which occur during growth, observation and analysis of the nuclei formed during growth, and the electronic properties of the nuclei and the substrate surface. STM analysis of diamond and diamond-like materials has been described in several recent studies. Previous works using STM by the authors have examined topography of CVD doped diamond films and undoped nuclei, changes in the growth surface and nuclei during growth, and examination of Ni contacts to single crystal diamond. [4-7] T. Tsuno and others have examined homoepitaxial CVD diamond films grown on the diamond (001) surface and observed surface reconstructions. [7] M. P. Everson et al have investigated the structure of doped nuclei grown on silicon. [8] The only group to report successful STM examination of thick undoped diamond films has come from H. G. Busmann et.al. [9] Several other groups have examined amorphic diamond and diamond-like carbon. [10-14] Discusions of the theory and practice of imaging diamond can be found in these references.

The changes in the surface which occur during growth can be examined before the first observation of nucleation. Figure 1 shows the surface structure of one of the samples as viewed by STM. Comparisons of the 30 minute and the 60 minute growth samples showed that the surface of the 60 minute sample appeared to be rougher than the 30 minute sample. Neither sample showed diamond nucleation. The surface, however, showed an increased roughness for the longer growth. This indicates the formation of a surface layer, presumably SiC or disordered carbon.

During the initial phase of the growth process examined here, a majority of nuclei exhibit a 3-dimensional structure. A minority of the nuclei do exhibit a more 2-dimensional structure, which indicates a 2-dimensional growth mode. Figure 2 shows both flat and hillocked structures characteristic of 2-dimensional and 3-dimensional growth modes, respectively. The top of the flat nucleus shown is smooth to within ~20Å and has a "height" to "width" ratio of 1:4. The surface of the nucleus is parallel to the substrate and indicates that the interactions with the substrate contribute to the growth and morphology. This is an important aspect because it is likely that the initial diamond has formed in the scratched regions. We would suggest that it is possible that the initial diamond formation in the scratches is highly disordered, thus allowing the substrate interactions to contribute to determination of the growth morphology. The second image shows several nuclei, one of which appears to be twinned, which have "height" to "width" ratios of ~1:2. The fact that both types of nuclei were observed after the same exposure to growth, supports the fact that two distinct modes exist and that the 2-D mode is not merely an early manifestation of a 3-D growth mode. Evidence of this 2-dimensional mode is interesting because it may be an indication that conformal growth is possible and if it could be enhanced, creating planer diamond films with fewer polycrystaline

domains might be possible.

Tunneling spectroscopy measurements show distinct I-V characteristics of the nuclei and the substrate. Examples of I-V curves obtained from different points are shown in Figure 3. The ability to distinquish between the types of materials on the surface is an important one. The curve obtained by tunneling to the diamond nucleus is smoothly varying and shows little response at positive bias voltages. The substrate I-V curve shows much more structure including a large change in the current starting at +2.5 volts. The "peaks" in the I-V curve taken over the substrate are indicative of the electronic structure of the carbonic layer that has formed on the substrate during growth. These "peaks" may be a result of absorbates, bonded to the silicon, which are weakly connected to bulk states.

The ability to carry out tunneling experiments from undoped diamond regions is in itself unique since diamond has such a high electrical resistivity. To probe the defect and impurity properties of the initial stages of growth, micro-photoluminescence measurements were carried out as a function of growth time. In this experiment, the same sample was measured after various growth times. A relatively strong feature was observed in the micro-photoluminescence at an emission energy of 1.68eV, which is shown in Figure 4. There has been considerable discussion about the origin of this feature. It occurs at an energy near to that of the GR1 peak in single crystal diamond. This feature has been assigned to a neutral vacancy. Since vacancies are mobile in diamond at temperatures ~800°C, it is unlikely that the 1.68eV feature in the CVD films (growth temperature ~800°C) is due to a vacancy. It has also been suggested that the feature is due to a complex involving Si and/or N.[15,16]

The results of the experiment are shown in Figure 5. The relative intensity of the 1.68eV feature to the Raman diamond feature reaches a maximum after ~7hr and then is reduced with increased growth time. The absolute intensity of the 1.68eV feature actually increases at least up to a growth time of 15 hrs (at this time the substrate is nearly completely covered). Thus we can conclude that there is initially a higher rate of impurity incorporation in the film. From the data, it can also be concluded that a higher concentration of defect centers exists near the interface between the diamond and the silicon, with a lower concentration found in the bulk. It is now well established that Si is etched in the presence of atomic H, with SiH_4 being released. We suggest that the observed photoluminescence trend is due to the incorporation of Si which has been etched from the substrate. The rate of incorporation decreases when the Si substrate is covered by diamond after subsequent growth.

B. Schottky Barrier Height Measurement

Diamond-metal interfaces and their properties as electrical contacts have received recent attention, and both ohmic and rectifying contacts to both natural diamond and CVD grown diamond have been reported [6,17-21]. To fully understand the rectifying contact it is

necessary to determine the Schottky barrier characteristics. Current-voltage measurements of the rectifying contacts typically show a high ideality factor and cannot be used for an accurate Schottky barrier determination [22]. Photoemission, however, has been successfully used to measure the Schottky barrier height of Al and Au on diamond [23].

Previous current-voltage measurements have demonstrated that titanium, deposited at room temperatures, forms a rectifying contact to p-type diamond. Upon annealing to >400°C the current-voltage characteristics become ohmic.[21]. It has been suggested that this transformation is due to the formation of a titanium carbide [17]. In a previous study we have shown that titanium carbide formation does indeed occur in the same temperature range in which titanium contacts are found to change from rectifying to ohmic [24]. In this paper we report a UV photoemission study of thin titanium layers deposited on a diamond (111) surface. From the measurements the Schottky barrier height of titanium on p-type diamond (111) is determined.

The Schottky barrier height of a metal on a p-type semiconductor is defined as the difference between the valence band edge of the semiconductor and the Fermi level of the metal at the interface. The determination of the Schottky barrier height from UV photoemission, relies on the fact that features of both the metal and the underlying semiconductor are visible in one spectrum. Experiments are therefore limited to thin metal films with a thickness on the order of the mean free path of the electrons (~5Å). Even at metal coverages less than the mean free path, it is not always possible to determine the position of the valence band edge accurately from the spectra, since emission from the metal d-band obscures the relatively weak semiconductor valence band emission. In those cases, a more accurate determination can be made, by relating the valence band edge to a feature in the diamond spectra that does remain visible at higher metal coverages. In this analysis it is assumed that shifts in the diamond features are uniform so that relative positions are maintained. In the experiments on the (111) surface, the valence band edge was determined from the spectrum of the argon plasma cleaned diamond and related to a stronger emission feature at lower energies, labeled B, in Figure 6. Although this diamond feature was attenuated upon metal coverage, it remained much more visible than the valence band edge. In order to determine the valence band edge from the position of peak B, their relative positions should not change upon titanium deposition. Since the relative positions of feature B and the valence band edge did not change after the first metal depositions in which both were visible, we do not expect this to occur at the higher metal thicknesses.

The location of the valence band edge was determined by extrapolating the spectrum to zero, as illustrated in Figure 7. The valence band edge was found to be 8.2 eV above feature B. After the first titanium deposition the diamond spectrum shifted 0.5 eV towards lower energies, indicating a change in the pinning position of the Fermi level in the gap. No Fermi

level emission due to the titanium could be discerned, however, at this coverage. Upon further titanium deposition, emission from the d-bands of titanium became pronounced, and the Fermi level could be clearly discerned. The position of the valence band edge, however, became more difficult to locate. Based on the position of feature B, no further shifts in the diamond spectrum were observed. This indicates that the Fermi level was pinned, and the Schottky barrier height established, after the first titanium deposition. The Fermi level was found to be 9.2 eV above feature B. Since the valence band edge was 8.2 eV above B this results in a Schottky barrier height for titanium on p-type diamond (111) of 1.0±0.2 eV.

Similar measurements were performed for titanium on the diamond (100) surface, as shown in Figure 8. The position of the valence band edge, relative to peak B, was determined again from the clean diamond (100) surface, and was found to be 8.0 eV, in agreement with the value found from the (111) surface. No shifts were observed before cleaning, and no significant shifts occurred upon titanium deposition. The position of the Fermi level was determined, and found to be 9.4 eV above feature B. The Schottky barrier height of titanium on the diamond (100) surface was therefore found to be 1.5±0.2 eV. Reported values for the Schottky barrier height of titanium on CVD grown diamond films range from 0.9(+0.5/-0.2)eV [24] to 1.3 eV [25].

C. Negative Electron Affinity

The relation between the bands of a semiconductor and the vacuum level can be described by the electron affinity. This quantity which is the energy difference between the conduction band minimum and the vacuum level, is an important parameter in the Schottky-Mott model for Schottky barrier heights. The electron affinity is however dependent on the surface structure of the crystal. A dipole layer on the surface will shift the potential of the material with respect to the vacuum, thus changing the electron affinity. The dipole layer can result from surface structures such as reconstruction or molecular absorption or interface structures such as Schottky barriers or heterojunctions.

Photoemission spectra of negative electron affinity surfaces generally show a sharp peak at the low kinetic energy end of the spectrum. This peak is attributed to emission of electrons that are quasi-thermalized to the bottom of the conduction band of the semiconductor. For materials with a positive electron affinity, the conduction band minimum is below the vacuum level, and the quasi-thermalized electrons are trapped in the sample. In the experiments described here, the presence of a sharp peak at the onset of the photoemission will be considered as an indication of a negative electron affinity surface.

Hydrogen Terminated Surfaces.

We initiated the study of the negative electron affinity of diamond by verifying the experiment of Pate [26] in which the relation between the negative electron affinity effect and the presence of hydrogen on the surface is established. The H-terminated surfaces were obtained by polishing and etching a diamond (111) wafer. Followed by a low temperature anneal (350°C) to desorb contaminants. Photoemission spectra from the diamond before and after thermal desorption of the hydrogen are shown in Figure 9. The negative electron affinity of the surface, which results in the sharp peak at the low energy end of the spectrum, has clearly been removed from the surface. Since the annealing temperature used to obtain the effect is the same as the reported temperature for the desorption of hydrogen, this suggest that hydrogen on the surface plays a role in the negative electron affinity effect. The spectra of the diamond before and after annealing, are followed by spectra from the diamond after exposure to molecular and mono-atomic hydrogen. As is shown in Figure 9, the molecular hydrogen has no effect on the electron affinity of the surface. The mono-atomic hydrogen, however, returned the surface to a negative electron affinity state. The fact that exposure to mono-atomic hydrogen causes the surface to exhibit a negative electron affinity confirms that the hydrogen is associated with the negative electron affinity. The difference between the results after exposure to molecular and mono-atomic hydrogen suggest that the hydrogen has to be chemically bonded to the surface. The series is concluded by a spectrum of the diamond after another high temperature anneal, which shows that the cycle is repeatable.

In a second series of experiments, described in Figure 10, the diamond (111) was exposed to a hydrogen plasma after loading, and the spectrum shows the presence of a negative electron affinity. After a subsequent exposure to an argon plasma, however, the sharp peak that is associated with a negative electron affinity, was absent. Since the negative electron affinity is associated with the presence of hydrogen on the surface we conclude that the argon plasma removed the hydrogen from the surface. Exposure to another hydrogen plasma causes the negative electron affinity effect to reappear. This is to be expected in light of the first experiment where exposure to mono-atomic hydrogen also caused the negative electron affinity to reappear.

Metal Induced Negative Electron Affinity.

The potential of metals inducing a negative electron affinity were explored. In this case the initial starting surface was a diamond (111) surface treated with a remotely excited Ar plasma to induce a surface with a slightly positive electron affinity. After the first titanium dose a sharp peak, similar to the one found on the hydrogen passivated diamond (111) surface, develops at the low energy end of the spectrum. In the same spectrum a 0.5 eV shift towards lower energies is observed. For increasing titanium coverages the peak is attenuated, and no further shifts in the diamond features are observed. We attribute this peak to a titanium induced

negative electron affinity. This would be due to a lowering of the work function by the titanium, as illustrated in Figure 11. Before the titanium deposition the Fermi level at the surface is 0.5 eV above the valence band edge. The vacuum level was determined from the low energy cutoff point of the emission, and is found to be about 5.5 eV above the valence band edge. Using a value of 5.45 eV for the bandgap of diamond we find therefore the vacuum level to be ~0.05 eV above the conduction band edge; electrons that are quasi-thermalized to the bottom of the conduction band are therefore unable to escape the surface. After the first sub-monolayer of titanium is deposited, the Fermi level is pinned at 1.0 eV above the valence band edge, which is the Schottky barrier height described in the previous section. The effective work function of the surface is now determined by the work function of the titanium. Using the value of 4.33 eV for the work function of bulk titanium [27] we find that the vacuum level of the surface is now located 0.2 eV below the conduction band edge and quasi-thermalized electrons can escape, causing the sharp peak in the spectrum. The fact that this peak is due to the interface of the diamond and the titanium, can be deduced from the attenuation of the peak as a function of coverage. Note that in this model the Schottky barrier height plays an important role in determining the position of the vacuum energy level. In Figure 10.b. the titanium-diamond(100) interface is described. Here the Schottky barrier height is 1.5 eV and the vacuum level lies now above the conduction band edge. Based on this model we do not expect a negative electron affinity surface. This is supported by the data, as can be seen in Figure 8. No low energy peak appears upon titanium coverage. It should be noted, that the model presented here, is the reverse from the Schottky-Mott model. There the Schottky barrier height is determined by aligning the vacuum levels of the metal and the semiconductor.

IV Conclusions

The initial stages of diamond growth show both substrate interactions which lead to non-diamond structures and diamond nuclei which form at scratches on the surface. Even though the initial diamond formation occurs in the scratches, the nuclei growth morphology is related to the substrate. We propose that the initial diamond formation is highly disordered and that as the growth proceeds beyond the scratches, the substrate interactions contribute to the growth morphology. Because of the high resistivity of undoped diamond, tunneling to these structures was not anticipated. Defect structures were observed in the microphotoluminescence measurements. These defects were apparently associated with Si impurities which were due to etching of the exposed substrate.

From the UV photoemission spectroscopy measurements presented here, a Schottky barrier height of 1.0±0.2 eV was found for the titanium-diamond (111) interface, and 1.5±0.2 eV for the titanium-diamond (100) interface It was found that the Schottky barrier heights were

established for sub-monolayer titanium coverages. Upon titanium deposition on the diamond (111) surface, a sharp (0.5 eV FWHM) peak developed at the position of the conduction band edge. This is indicative of a negative electron affinity surface. Negative electron affinity surfaces are commonly obtained on III-V semiconductors by depositing a thin layer of a low work function material such as cesium or cesium-oxide. This study shows that it is possible to obtain a negative electron affinity on diamond (111) by depositing a sub-monolayer of a titanium, and suggests the possibility of inducing a negative electron affinity on diamond using other transition metals. A model for the observed negative electron affinity was presented, based on the Schottky barrier height of the diamond-metal interface, and the work function of the metal.

Acknowledgments: We thank B. Stoner and J.T. Glass for providing the initial diamond growth films, K. Das of Kobe Research for his help in establishing the diamond cleaning procedure, T. P. Schneider for the plasma cleaning work, and R. Rudder and R. Markunas of RTI for helpful discussions. This work is supported in part by the ONR through grants, N00014-92-J-1477, N00014-90-J-1604, N00014-90-J-1707, the NSF through grant DMR 9204285, and the MITI of Japan through the NEDO program.

References

1. R.J. Nemanich, Annu. Rev. Mater. Sci. **21**, 535 (1991).
2. B.R. Stoner and J.T. Glass, Appl. Phys. Lett. **60**, 698 (1992).
3. S. Koizumi, T. Murakami, T. Inuzuka, and K. Suzuki, Appl. Phys. Lett. **57**, 563 (1990).
4. K. F. Turner, B. R. Stoner, L. Bergman, J. T. Glass, and R. J. Nemanich, J. Appl. Phys. **69**, 6400 (1991).
5. K. F. Turner, Y. M. LeGrice, B. R. Stoner, J. T. Glass, and R. J. Nemanich, J. Vac. Sci. Technol. B. **9**, 914 (1991).
6. T. P. Humphreys, J. V. LaBrasca, R. J. Nemanich, K. Das, and J. B. Posthill, Jpn. J. Appl. Phys., Pt. 2 **30**, 1409 (1991).
7. T. Tsuno, T. Imai, Y. Nishibayashi, N. Fujimori, and K. Hamada, Jpn. J. Appl. Phys., Pt. 1, **30**, 1063 (1991).
8. M. P. Everson, and M. A. Tamor, J. Vac. Sci. Technol., B. **9**, 1570 (1991).
9. H. G. Busmann, and H. Sprang, I. V. Hertel, W. Zimmermann-Edling, H. J. Guentherodt, Appl. Phys. Lett. **59**, 295 (1991).
10. J. A. Martin, L. Vazquez, P. Bernard, F. Comin, and S. Ferrer, Appl. Phys. Lett **57**, 1742 (1990).
11. C. B. Collins,F. Devanloo, D.R. Jander, T.J. Lee, H. Park, and J.H. You, J. Appl. Phys. **69**, 7862 (1991).
12. S. Ferrer, F. Comin, J. A. Martin, L. Vazquez, and P. Bernard, Surf. Sci. **251/252**, 960 (1991).
13. C. B. Collins, F. Davanloo, E. M. Juengerman, D. R. Jander, and T. J. Lee, Surf. Coat. Technol. **47**, 754 (1991).
14. N. H. Cho, D. K.Veirs, J. W. Ager III, M. D. Rubin, C. B. Hopper, and D. B. Bogy, J. Appl. Phys **71**, 2243 (1992).
15. A.T. Collins, M. Kamo, and Y. Sato, J. Mater. Res. **5**, 2507 (1990).
16. J. A. Freitas, Jr., J. E. Butler, and U. Strom, J. Mater. Res. **5**, 2503 (1990).
17. G. S. Gildenblat, S. A. Grot, C. W. Hatfield, A. R. Badzian, and T. Badzian, IEEE Elect. Dev. Lett. **11**, 371 (1990).
18. K. L. Moazed, R. Nguyen, and J. R. Zeidler, IEEE Elect. Dev. Lett. **9**, 350 (1988).
19. H. Shiomi, H. Nakahata, T. Imai, Y. Nishibayashi, and N. Fujimori, Appl. Phys. (part I) **28**, 758 (1989).
20. J. W. Glesener, and A. A. Morrish, K. A. Snail, J. Appl. Phys. **70**, 5144 (1991).
21. K. L. Moazed, J. R. Zeidler, and M. J. Taylor, J. Appl. Phys. **68**, 2246 (1990).
22. M. C. Hicks, et al., J. Appl. Phys. **65**, 2139 (1989).
23. F. J. Himpsel, P. Heimann, D. E. Eastman, Solid State Comm. **36**, 631 (1980).

24. J. van der Weide and R. J. Nemanich, *Proceedings of the First International Conference on the Applications of Diamond Films and Related Materials*, edited by Y. Tzeng, M. Yoshikawa, M. Murakawa and A. Feldman. (Elsevier, New York, 1991), p.359.
25. T. Tachibana, B.E. Williams, and J.T. Glass, Phys. Rev. B, (in press).
26. B.B. Pate, M.H. Hecht, C. Binns, I Lindau, and W.E. Spicer, J. Vac. Sci. Technol. **21**, 364 (1982).
27. E.H. Rhoderick, and R.H. Williams, Metal-Semiconductor Contacts, (Clarendon press, Oxford, 1988).

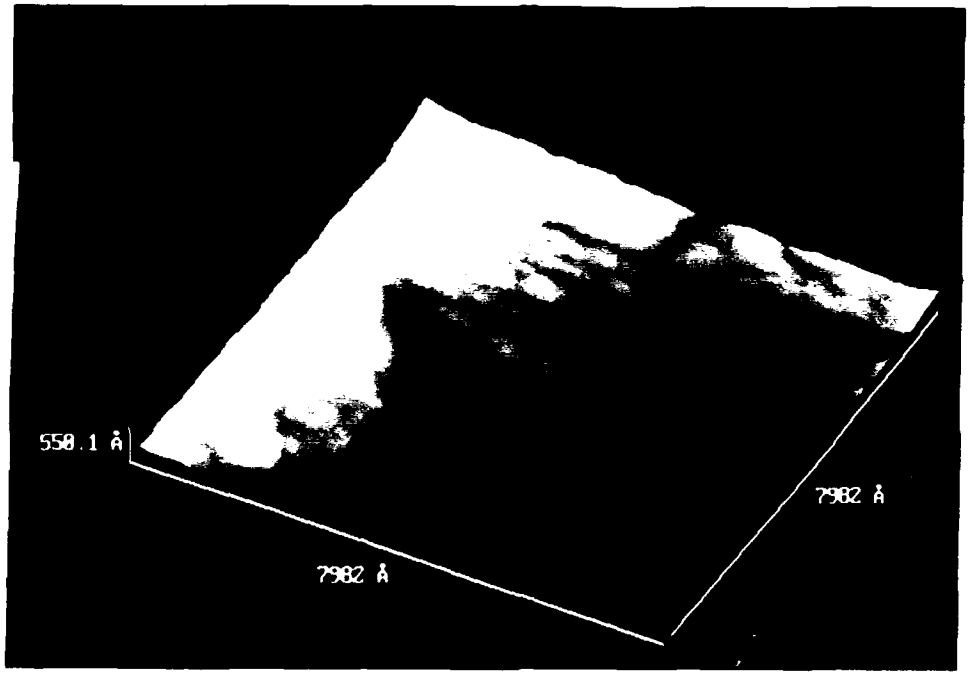

Figure 1 STM micrograph of the scratched Si surface after 60 minute exposure to plasma growth conditions. Scratches can be seen on the substrate which have been used to increase the nucleation density. The roughness of this sample provides evidence of plasma induced surface modification preceeding diamond nucleation.

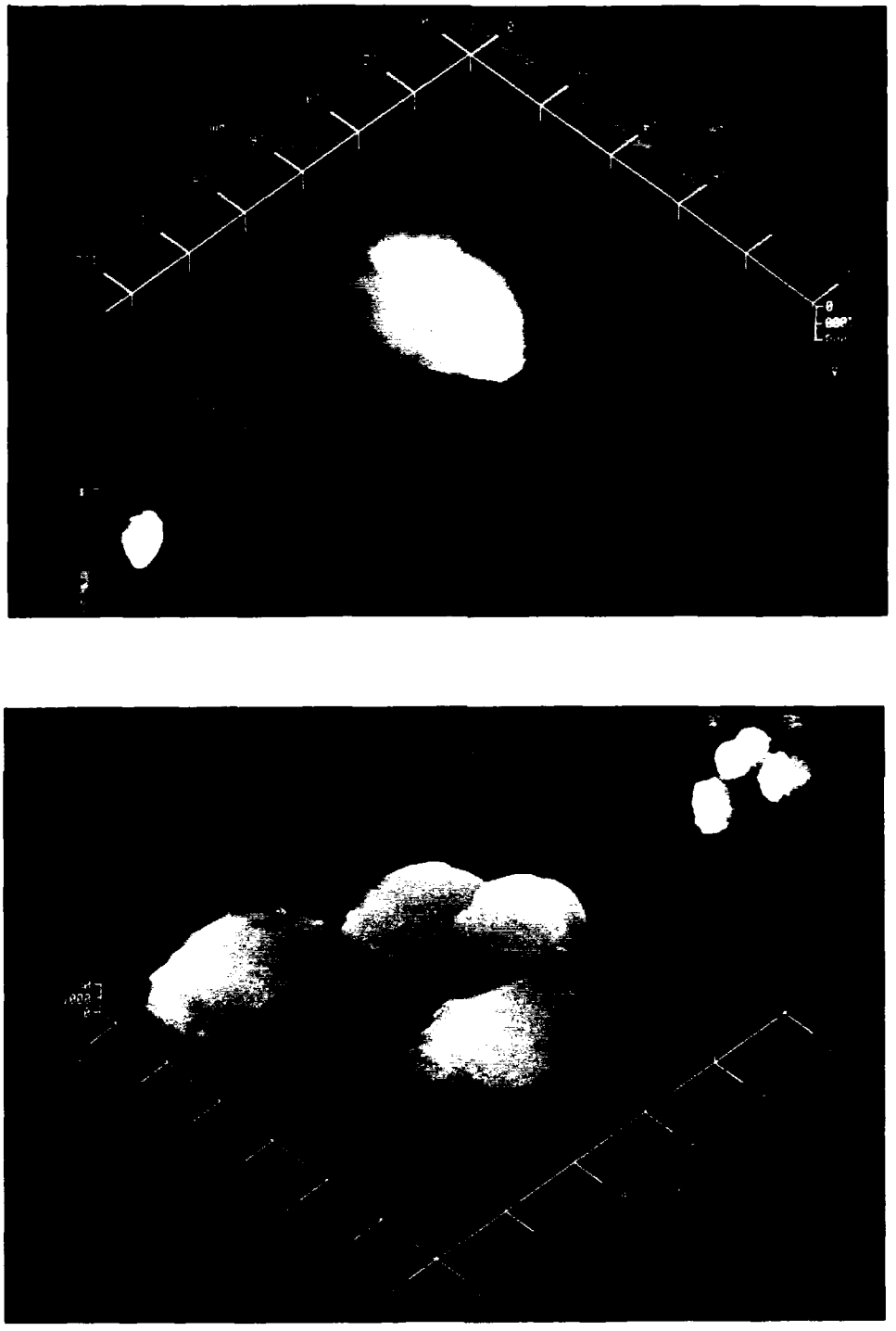

Figure 2 STM images of diamond nuclei on Si. The upper STM micrograph shows a nucleus of diamond grown on silicon that is exhibiting a flat surface nearly parallel to the substrate. The lower micrograph shows several nuclei that are growing 3-dimensionally. Both types of nuclei were found on the same silicon substrate after 1 hour of deposition.

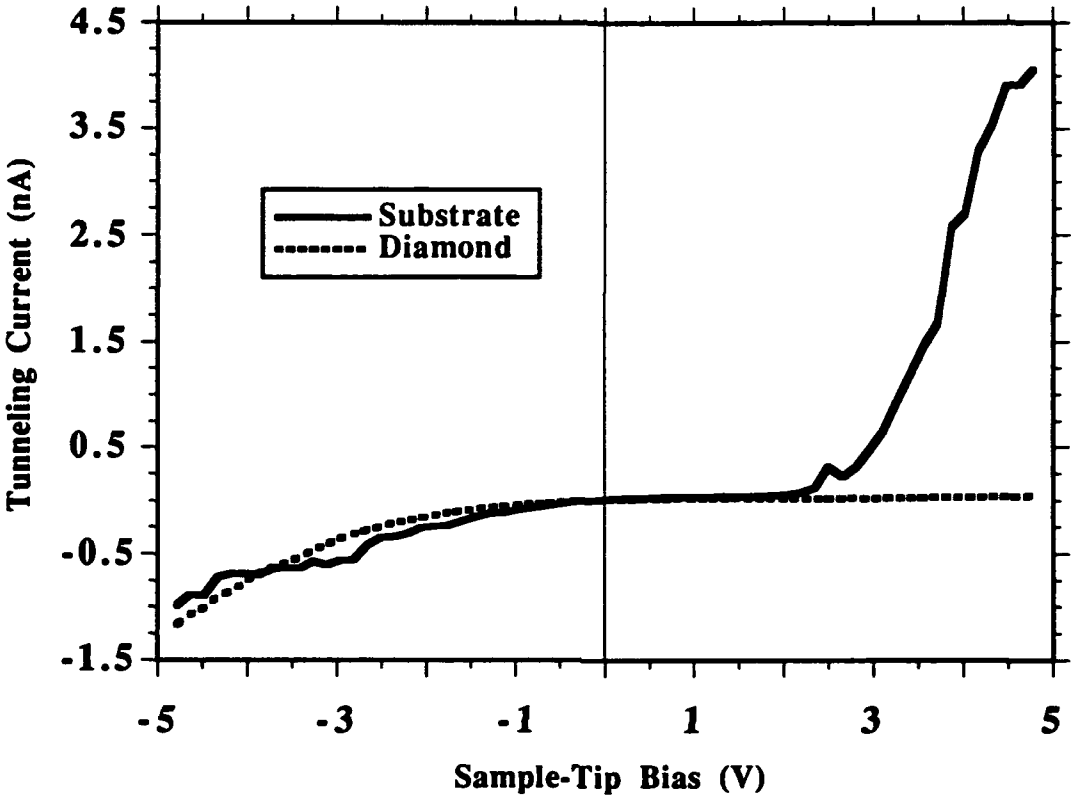

Figure 3 A comparison of the scanning tunneling spectroscopy current-voltage characteristics of a diamond nucleus and areas of the substrate near the nucleus.

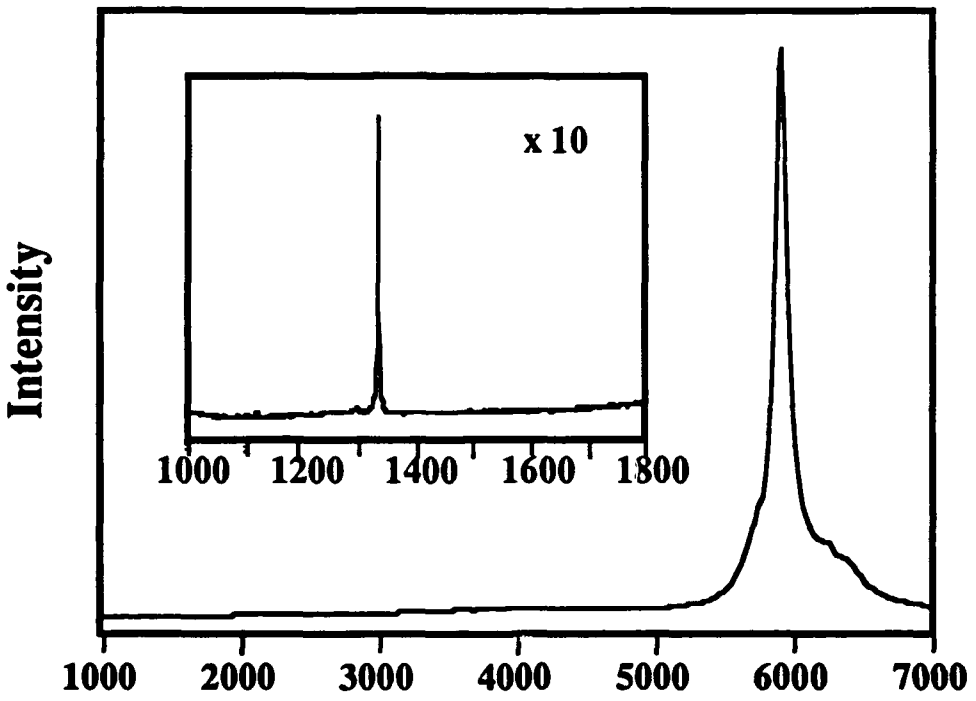

Figure 4 The Raman/photoluminescence spectrum of CVD diamond after 7 hours of growth. The spectrum was excited with 514.5 nm Ar ion laser light. The spectrum is domainated by the 1.68 eV photoluminescence center for a CVD diamond, and the inset shows an expanded higher resolution scan over the region of the diamond-sp2 Raman peaks. At this growth time, the emission from the 1.68 eV PL center showed a maximum relative to the intensity of the diamond Raman.

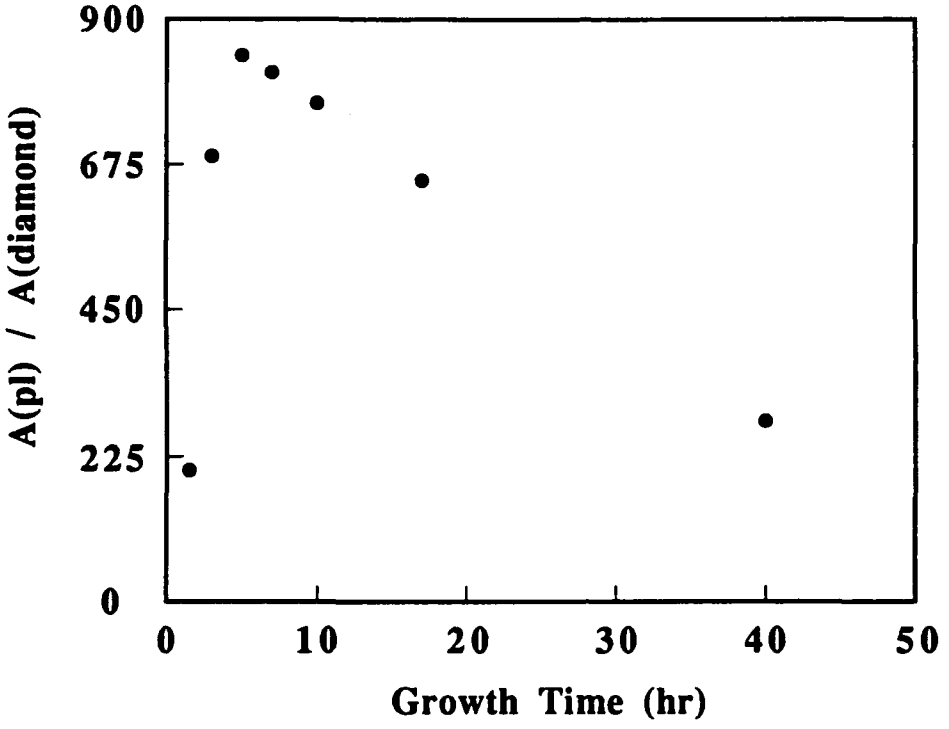

Figure 5 The integrated intensity of the 1.68 eV PL center relative to the diamond Raman peak as a function of deposition time. A maximum is observed after ~7 hours of growth.

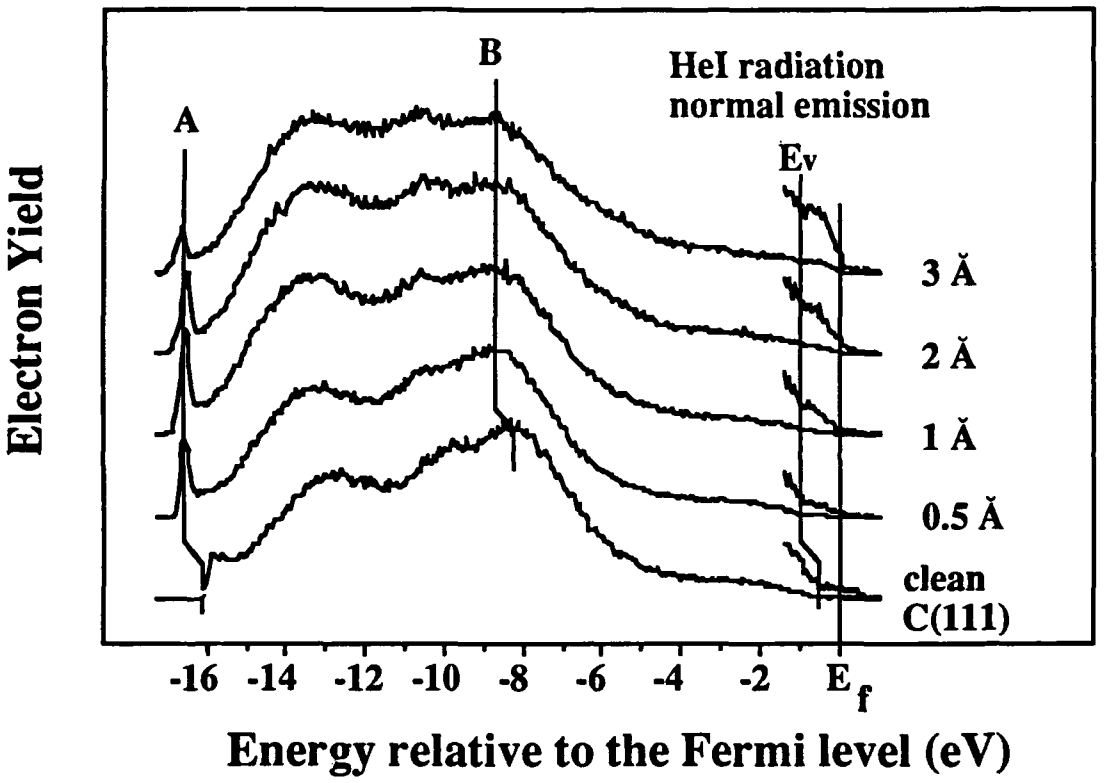

Figure 6. ARUPS spectra of titanium on diamond (111) for increasing titanium thicknesses. After the first deposition the spectrum shifts 0.5 eV toward lower energies and a sharp peak (A), indicative of a negative electron affinity, develops at the low energy cutoff. For increasing titanium thicknesses a Fermi level edge (Ef) develops, while at the same time the position of the valence band edge (Ev) becomes harder to locate. The Schottky barrier height is the energy difference between Ev and Ef

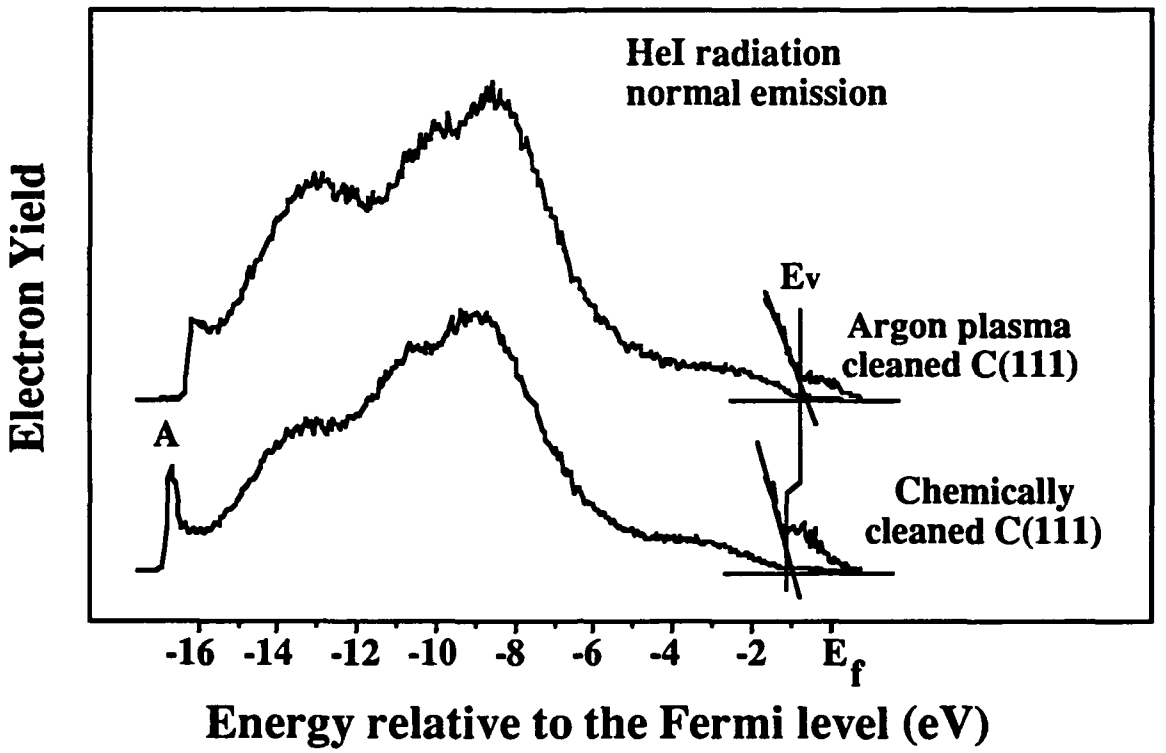

Figure 7. ARUPS spectra of diamond (111) before and after argon plasma cleaning. The spectrum shifts by 0.5 eV towards higher energies while the negative electron affinity peak (A) is significantly reduced after the argon plasma cleaning. The latter effect is attributed to the removal of hydrogen from the surface. The valence band edge is determined by linearly extrapolating the onset of emission down to zero.

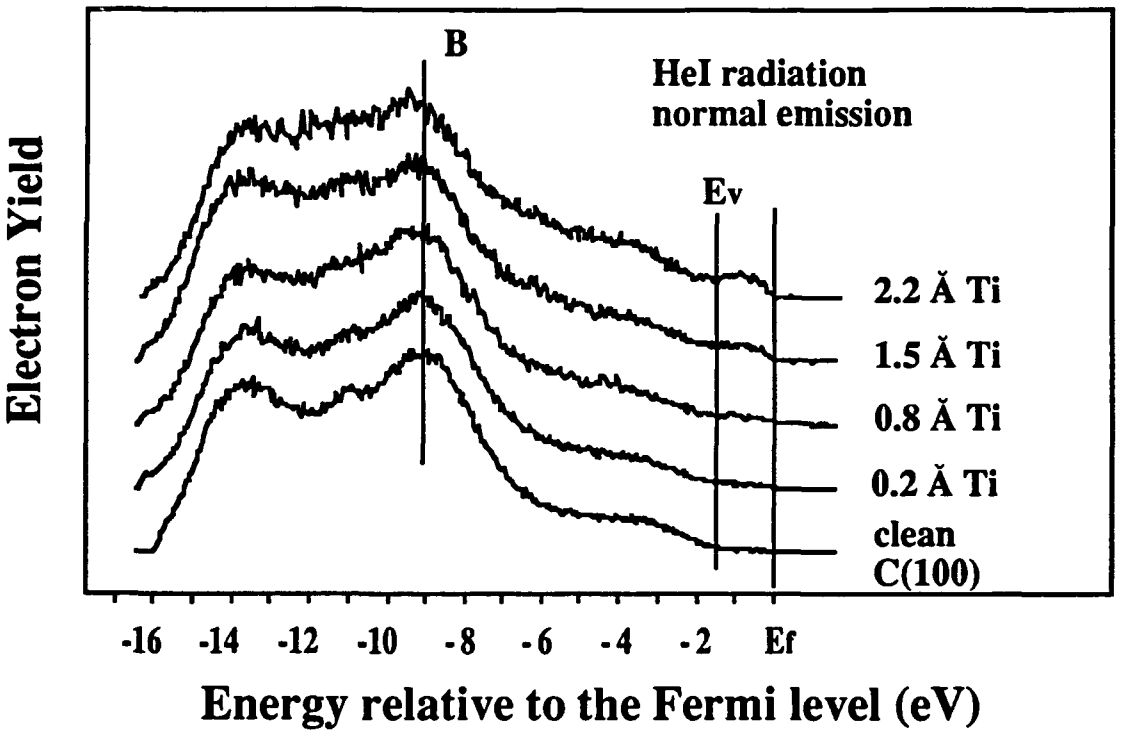

Figure 8. ARUPS spectra of titanium on diamond (100) for increasing titanium thicknesses. The position of Ev relative to peak B is determined from the clean surface and is found to be 8.0 eV. The Fermi level is found from the metal covered diamond (100) and lies 9.4eV above peak B, resulting in a Schottky barrier height of 1.5±0.2 eV.

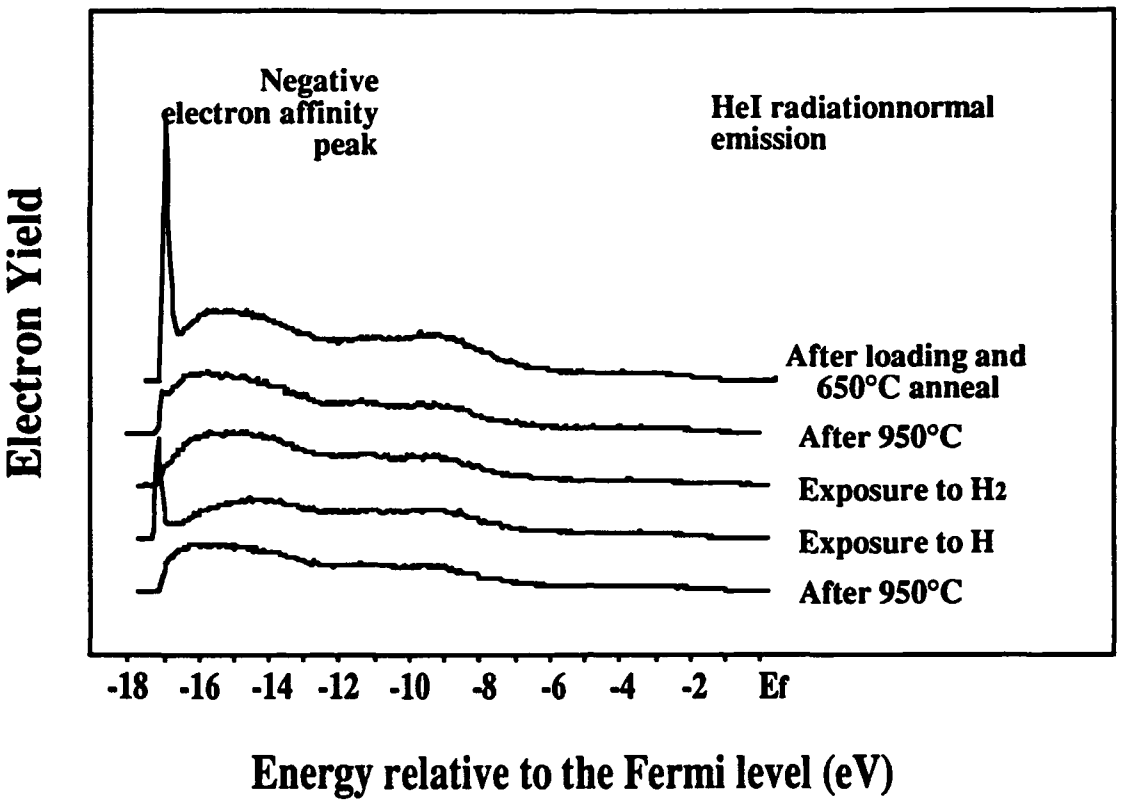

Figure 9 ARUPS spectra of diamond (111). The as loaded spectrum (top) shows the presence of a sharp peak at the lowest energy indicating a negative electron affinity. After a 950°C anneal the peak is gone, indicating the absence of a negative electron affinity. No significant changes occur after exposure to molecular hydrogen for 5 minutes at 10^{-6} Torr. After exposure to mono-atomic hydrogen however the negative electron affinity returns. The bottom spectrum, after another 950°C anneal, shows that the cycle can be repeated.

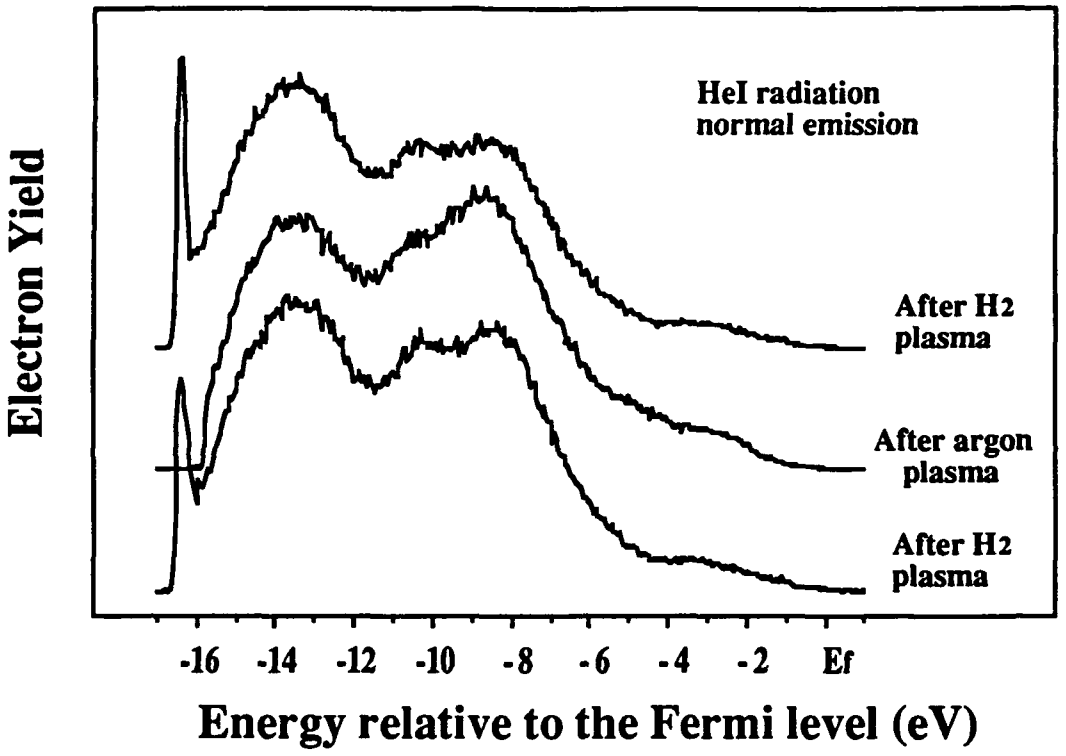

Figure 10. ARUPS spectra of diamond (111) after exposure to: from bottom to top, an hydrogen plasma, an argon plasma and a hydrogen plasma. The diamond was heated to approximately 350°C during each exposure. The spectrum after the first hydrogen plasma shows a sharp peak, due to the negative electron affinity of the surface. In the second spectrum, after argon plasma exposure, the peak is absent, indicating a positive or zero electron affinity. In the third spectrum the negative electron affinity is seen to reappear, after exposure to another hydrogen plasma.

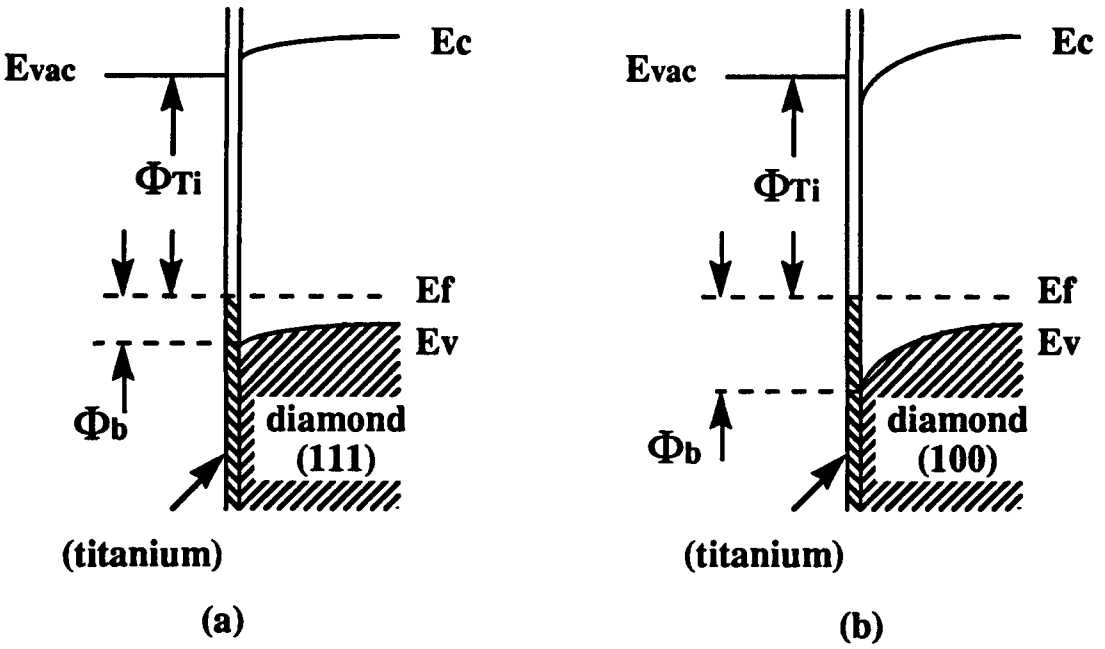

Figure 11. Model for the titanium induced negative electron affinity on diamond (111). In (a) the sum of the work function of the titanium (Φ_{Ti}) and the Schottky barrier height of titanium on the diamond (111) surface (Φ_{Ti}) is less then the bandgap of the diamond. This lowers the effective work function of the surface such that the conduction band minimum is above the vacuum level, thus resulting in a negative electron affinity. For the diamond (100) surface (b), however, the Schottky barrier height with the titanium is larger than the Schottky barrier height on the diamond (111) surface, and the sum of the Schottky barrier height and the work function of titanium is more than the bandgap of the diamond, resulting in a positive electron affinity.

IV. Modeling of Microwave MESFET Electronic Devices Fabricated from Semiconducting Diamond Thin Films

A. Introduction

The modeling effort on this program has previously considered the RF operation of diamond MESFETs and IMPATT diodes. Although the MESFET simulation work is continuing the modeling effort has been expanded and we are currently developing a simulation program to computationally investigate the suitability of both monocrystalline and polycrystalline diamond for Metal-Oxide-Semiconductor Field Effect Transistors (MOSFETs). The simulation program is now running and we have used it to predict dc and RF performance of FETs fabricated from both SiC and diamond. Preliminary dc simulations for diamond MOSFETs are presented in this report.

MOSFETs are of interest because metal-semiconductor interfaces are of poor quality, especially for polycrystalline diamond. Experimental p-type MOSFETs have been fabricated from naturally occurring single-crystal diamond that has been ion-implanted [2], from homo-epitaxially grown single crystal diamond [1], and from epitaxially grown polycrystalline diamond [5]. Boron is the acceptor in all of the devices. Previous simulations using the NCSU large-signal MESFET model [3] predicted substantial increase in output power for single crystal MESFETs [6] for the case of complete carrier activation. Although this approximation is reasonable for high temperature operation (i.e., T>500 °C), the assumption does not give a realistic estimate of free carrier density at room temperature.

The new code models incomplete activation and extends previous MESFET simulations to monocrystalline and polycrystalline MOSFETs.

B. Investigation Procedure

Our experimental approach is to replace the intrinsic FET model of TEFLON, the NCSU large-signal MESFET simulator [3] with a model of the MOSFET written in Pisces-II [4].

TEFLON combines a sophisticated analytic approximation of the physics in the gate region of a MESFET with harmonic balance to predict large-signal RF performance of realistic microwave circuits.

The physics of the diamond MOSFET channel is similar to the physics currently modeled by TEFLON for the GaAs MESFET. The questions of interest for large-signal or RF applications of diamond MOSFETs are also similar to those addressed by TEFLON, such as predicting gain as a function of input power, estimating power-added efficiency, and calculating output power into saturation. Realistic high-frequency simulation of a FET must include an embedding circuit, which we modeled conventionally as linear, lumped-element input and output microwave circuits. We use the harmonic balance routines of TEFLON to solve the nonlinear FET circuit simultaneously with the linear embedding circuit. In addition,

we include realistically adjusted values for parasitic elements around the intrinsic FET.

TEFLON is a quasi-static approximation that used dc values of currents and capacitances Id, Ig, Cgs, and Cds tabulated as function of the biases Vgs and Vds. These values are computed using Pisces IIB, accounting for incomplete carrier activation.

Pisces is a two-dimensional device modeling and simulation program developed at Stanford [4]. Pisces employs a finite-difference approach which is too slow to be directly interfaced with a harmonic balance routine. However, Pisces is well suited to analysis of dc device behavior, including the estimation of I-V curves and gate capacitances. Pisces supports some RF simulations with simple embedding circuits, but not the rich set of RF circuit simulations that TEFLON addresses.

We have developed a combined simulation program including Pisces to simulate dc I-V curves and other relevant dc behavior in the diamond MOSFET gate region, TEFLON to simulate RF behavior from dc I-V curves, and an interface between the two programs.

C. Results

We have tested the combined TEFLON-PISCES simulator on data from SiC FETs and we have validated the PISCES part of the simulator with dc measurements of three different diamond FETs:

1. a boron-doped homoepitaxially grown single-crystal device fabricated at Penn State [1].
2. an ion-implanted homoepitaxially grown single-crystal device fabricated at the Naval Ocean Systems Center (NOSC) [2], and
3. a boron-doped heteroepitaxially grown polycrystalline diamond fabricated at Kobe Steel Electronic Materials Center in North Carolina [5].

We have also considered a diamond JFET device.

The Penn State device reported by Grot, Gildenblat, and Badzian is a recessed gate naturally doped p-type MOSFET [1]. This device was fabricated using ECR plasma etching of an active layer. Most of the parameters required for the simulation were reported: oxide thickness of 100 nm, gate length of 5 micron, gate width of 30 micron, active layer thickness of 0.8 micron, recess depth of 0.2 micron. The doping concentration of the active layer was determined to be about 1.2×10^{16} cm^{-3}. This number corresponds to 0.1% hole ionization at room temperature.

The dc simulation was performed at a temperature of 473 °K so that a direct comparison with the experimental results could be performed. Because measured hole mobility of 280 cm^2/V-sec was given only at room temperature in the Penn State report, the mobility was adjusted for high temperature operation. Alternative physical models were considered and sensitivity to material parameters was numerically explored.

It was found that an incomplete ionization model was most critical for agreement between simulation and measured data. Good simulation of the diamond single-crystal device required a high value of acceptor energy level (Ea=0.37 eV). Figure 1 shows the I-V curve simulated at Vg=0 and Vg=70 v. The drain current at Vds=-50 v for zero gate bias and Vds=70 v are about 5.2 μA/μm and 2.8 μA/μm, respectively. These values are in good agreement with the experimental results of 3.8 μA/μm and 1.0 μA/μm, respectively.

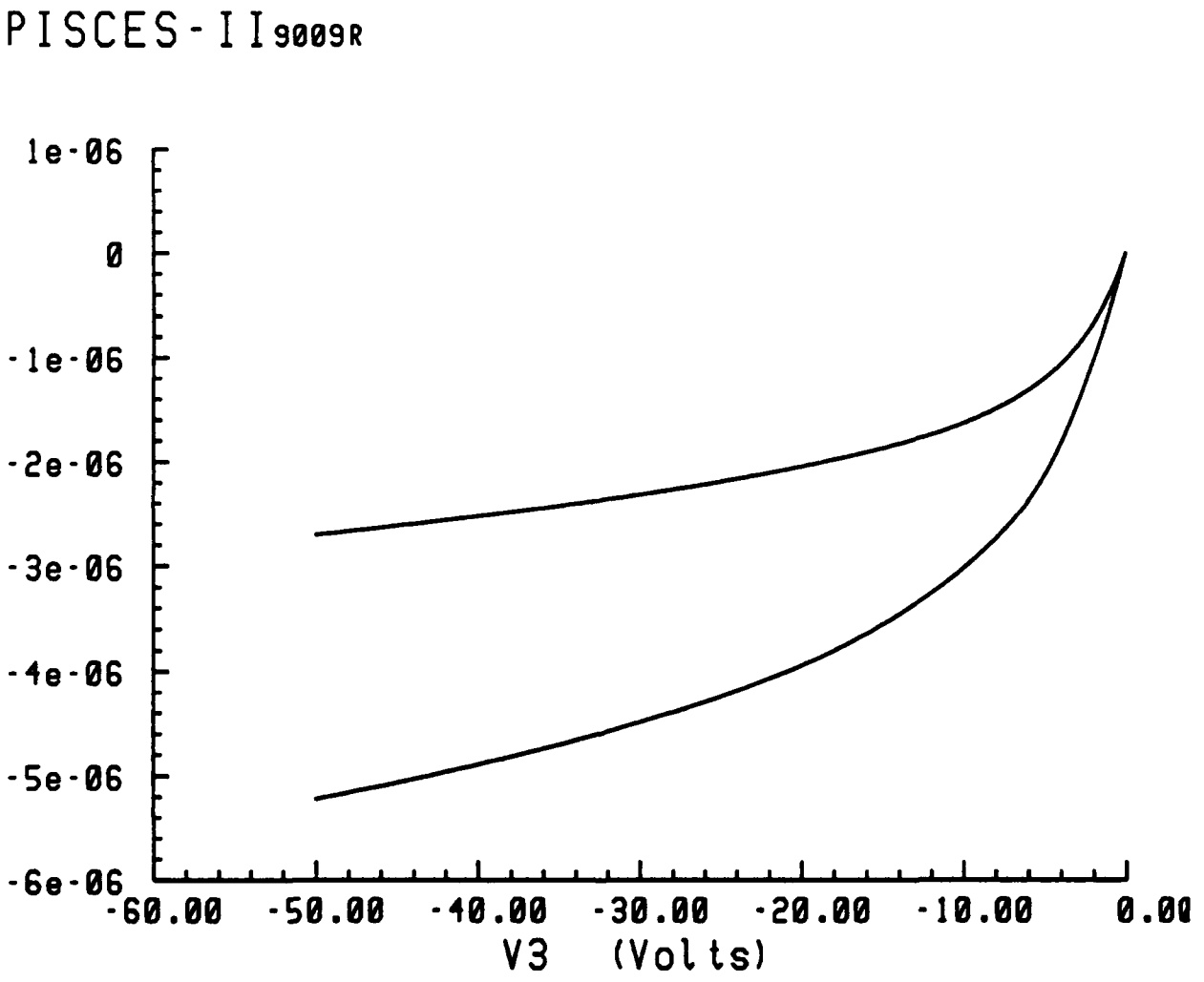

Figure 1. Drain Current versus Drain Voltage for the Penn State Device for Vg=70 v (top curve) and Vg=0 v (bottom curve).

The NOSC device reported by Hewett, et al. is an ion-implanted p-type Insulated-Gate FET fabricated from a single crystal thin film diamond, epitaxially grown on a naturally occurring diamond substrate [2]. A multiple implant scheme was used to provide an approximately uniformly doped active layer of about 210 nm in thickness. The device was fabricated in a concentric ring structure with 1000 μm wide gate in outer diameter (600 μm of inner diameter).

The gate length was 1 μm. All the materials parameters and physical model functions were the same as before, except that the room temperature free hole concentration and mobility were taken to be the measured values of 5×10^{15} cm^{-3} and 30 cm^2/V-sec, respectively.

The I-V characteristics at room temperature are shown in Figure 2. Current saturation is clearly observed. The simulated I-V curves agree with experiment, except for pinch-off. Pinch-off in the actual device was observed at a gate bias of approximately +12 v, but is harder to obtain in simulation. This may be due to our simple models of free carrier density and mobility in the multiply ion-implanted device. Actual doping profiles are not uniform. In future research, we will use optimization techniques to obtain more accurate and realistic values for the material parameters from the performance of the diamond devices.

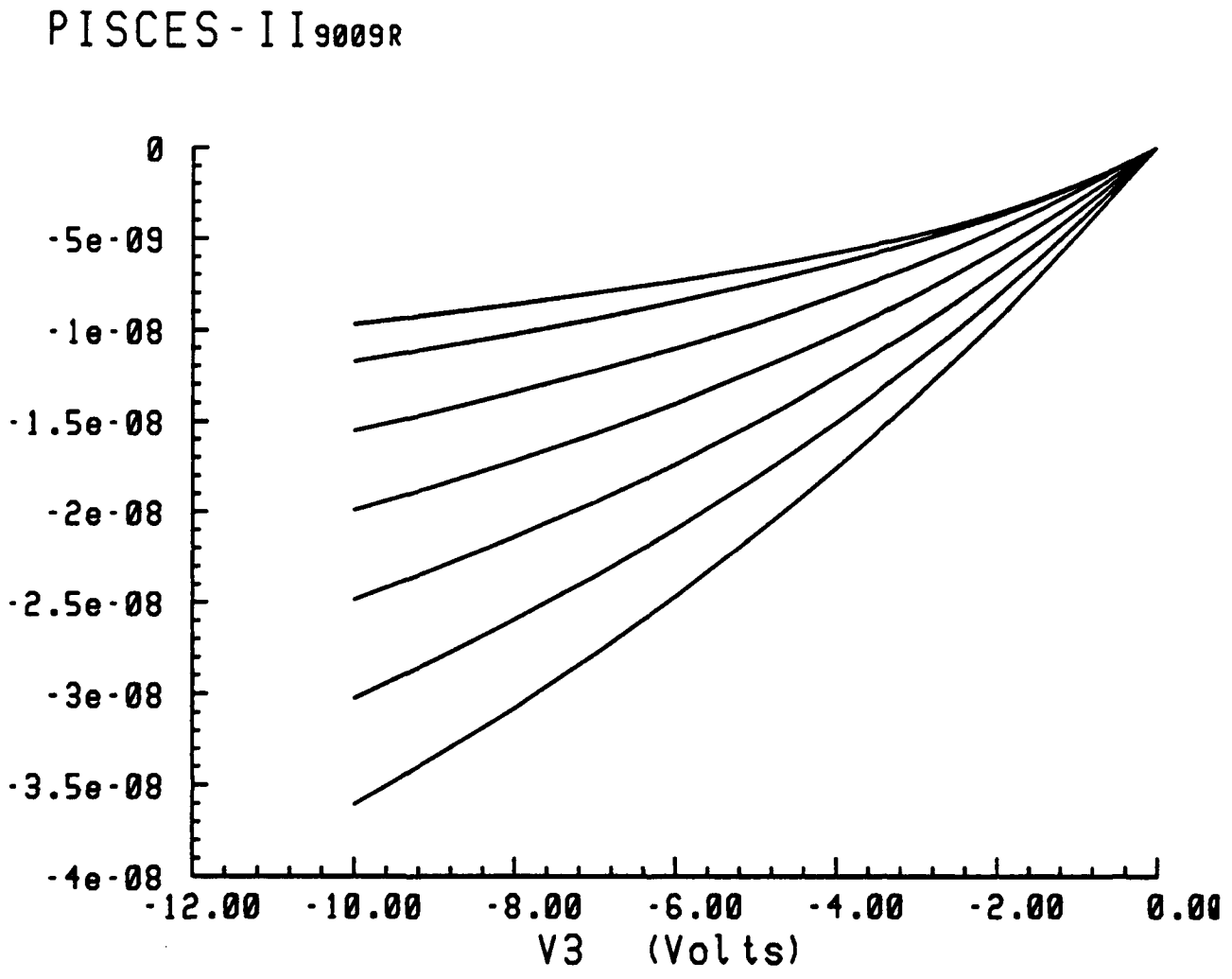

Figure 2. Drain Current versus Drain Voltage for the NOSC Device for Vg=12 v (top curve) to Vg=0 v (bottom curve) in Steps of -2 v.

The Kobe device reported by Tessmer et al. is a synthetic device [5]. This was the first device which exhibits saturation and pinch-off in a polycrystalline diamond FET. A 0.5 μm thick active layer of p-type diamond was grown by adding diborone in the gas phase. Boron concentration was measured to be about 7×10^{16} cm^{-3}. The device was fabricated in a concentric ring structure with nominal gate length of 2 μm and gate width of 314 μm.

The I-V characteristic at 423 °K shows pentode-like behavior, as indicated in Figure 3. The drain current is very low, about 10 pA/mm at Vg=0 v and Vds=-20 v. The simulated and measured data are in good agreement.

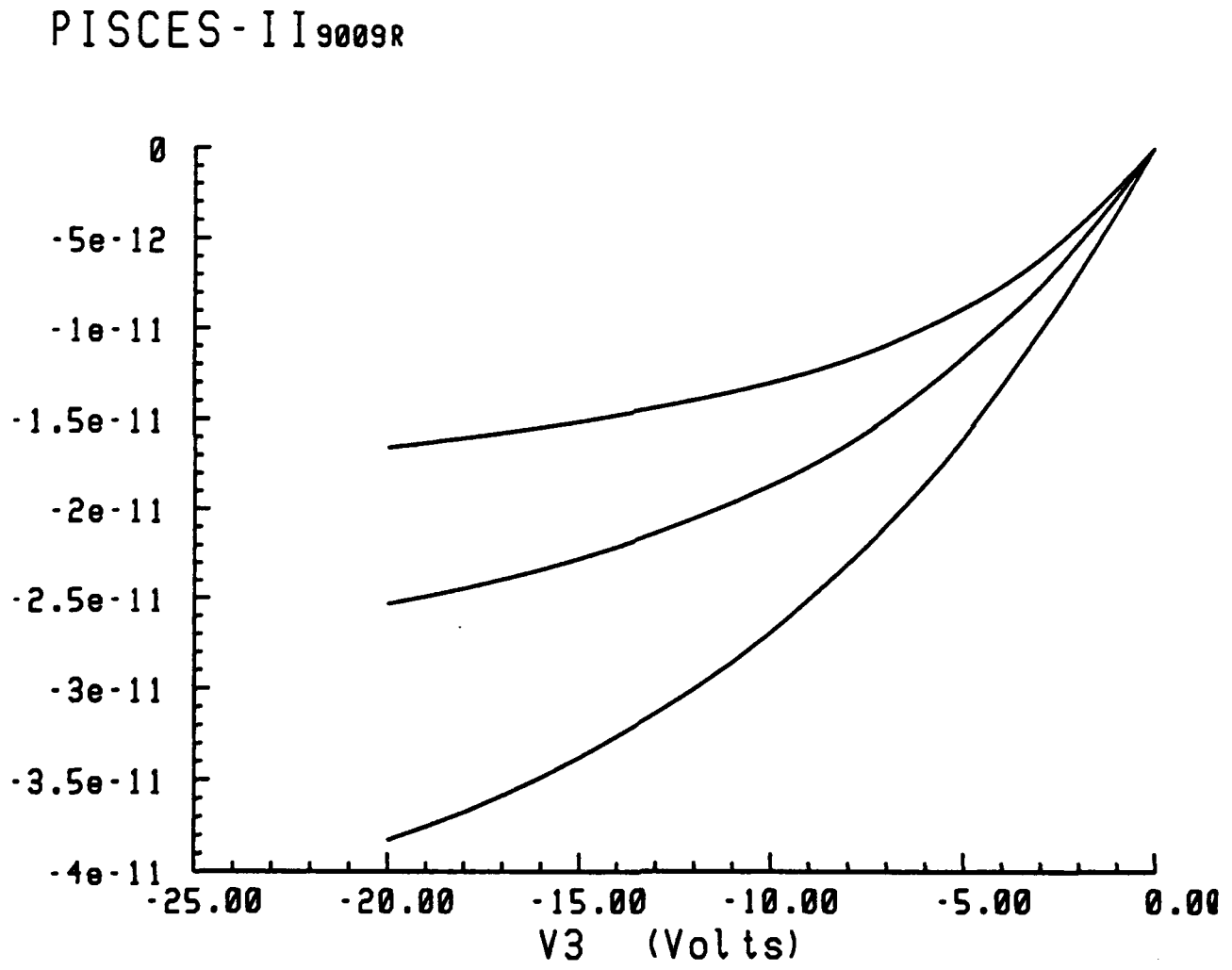

Figure 3. Drain Current versus Drain Voltage for the Kobe Device at T=423 °K for Vg=10 v (top curve) to Vg=0 v (bottom curve) in Steps of -5 v.

The simulations indicate that polycrystalline diamond may have an effective boron activation energy of about 0.65 eV, rather than the 0.37 eV expected for single crystal material.

The increase may be due to the trapping of carriers at the grain boundaries at doping concentrations of around 7×10^{16} cm^{-3}. This would indicate a barrier height at the grain boundary of about 0.3 eV in this device (grain size of 3 μm).

We have also conducted preliminary simulations of a diamond JFET assuming that an n-type dopant may be found. Figure 4 shows that at room temperature, the I-V characteristics of diamond JFETs shown strong space-charge limited behavior. At higher temperature, the behavior may become more pentode-like due to an increased number of free carriers. Also, the shape of the I-V curve is sensitive to the geometry of the channel, i.e., the gate length to the channel width ratio.

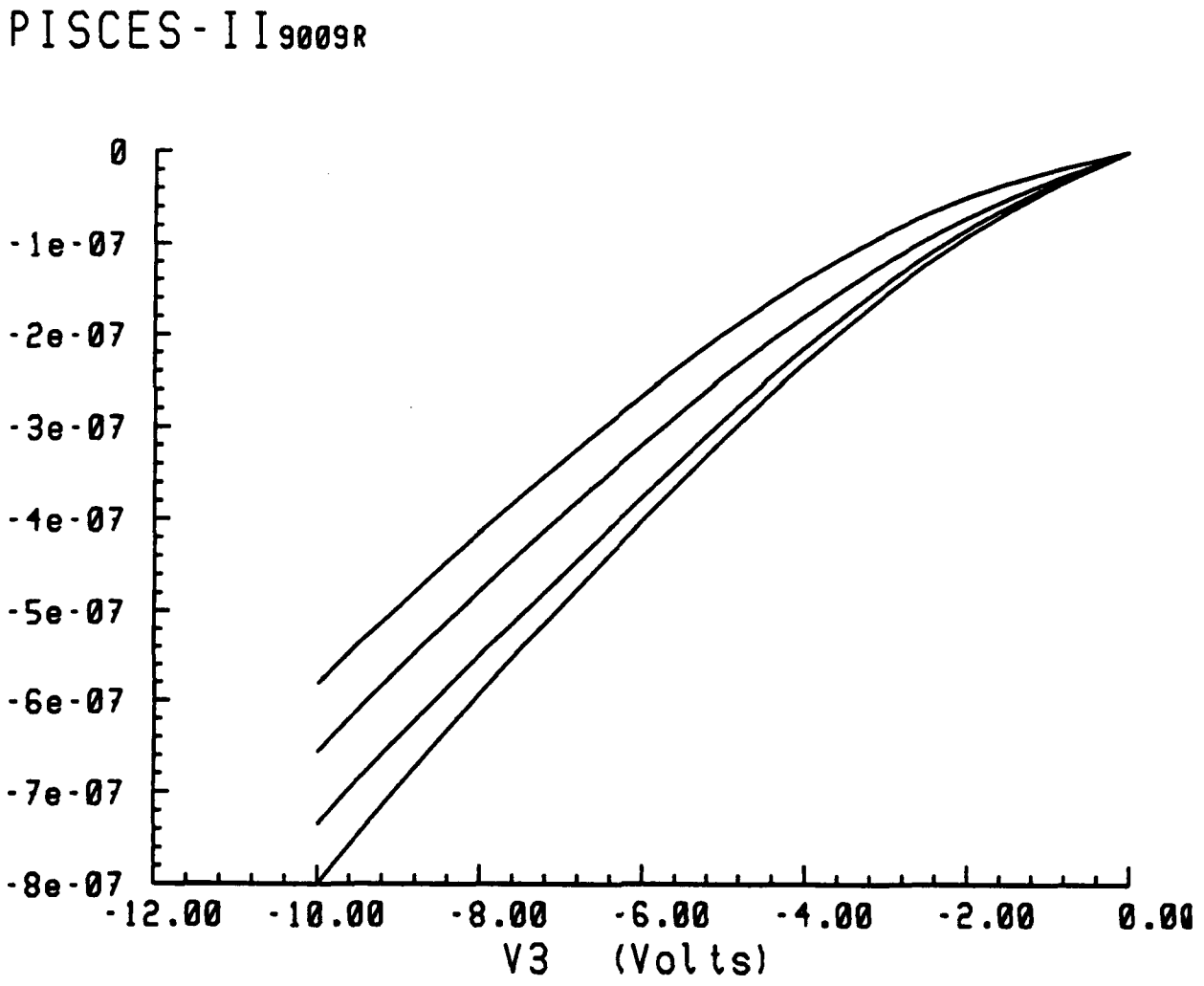

Figure 4. Triode-Like Drain Current versus Drain Voltage for the Diamond JFET for Vg=6 v (top curve) to Vg=0 v (bottom curve) in Steps of -2 v.

D. Discussion

Our simulated dc I-V curves for each device agree well with the corresponding

measurements as shown in the figures. We obtain pentode-like or triode-like behavior at the appropriate active carrier levels. The active carrier density depends upon doping level and temperature because of the dependence of activation on temperature.

There also appears to be significant dependence of the shape of the I-V curves on bound change at the interface because of backgating. Since bound charge depends upon processing and fabrication technology, the simulations may require recalibration for different fabrication processes.

E. Conclusions

It is possible to model polycrystalline and monocrystalline diamond FETs. The models confirm our understanding of the major physical processes in these devices. It is found that carrier activation and charge transport as a function of temperature are critical parameters in obtaining good agreement between simulated and measured data. Three different experimental diamond FETs were simulated and good agreement between the simulated and measured data was obtained in all three cases.

F. Future Research Plans and Goals

Single-crystal diamond MESFETs will be simulated in more detail. The effects of bound charge at the surface and the channel/substrate interface will be investigated. The RF operation of the devices over a range of operating temperatures will be examined.

G. References

1. S.A. Grot, G.S. Gildenblat, and A.R. Badzian, "Diamond Thin-Film Recessed Gate Field-Effect Transistors Fabricated by Electron Cyclotron Resonance Plasma Etching," *IEEE Electron Dev. Lett.*, **13**, pp. 462-464, 1992.
2. C.A. Hewett, C.R. Zeisse, R. Nguyen, and J.R. Zeidler, "Fabrication of an Insulated Gate Diamond FET for High Temperature Applications," *First International High Temperature Electronics Conf.*, pp. 168-173, 1991.
3. M.A. Khatibzadeh and R.J. Trew, "A Large-Sijgnal Analytic Model for the GaAs MESFET," *IEEE Trans. Microwave Theory Tech.*, vol. MTT-36, pp. 231-238, 1988.
4. M.R. Pinto, C.S. Rafferty, H.R. Yeager, and R.W. Dutton, "Pisces-II Technical Report," Stanford Electronics Laboratory, Stanford University, 1985.
5. A.J. Tessmer, L.S. Plano, and D.L. Dreifus, "Current Voltage Characteristics of In-Situ Doped Polycrystalline Diamond Field Effect Transistors," *Technical Report*, Kobe Steel, USA, Electronics Materials Division, 1992.
6. R.J. Trew, J.B. Yan, and P.M. Mock, "The Potential of Diamond and SiC Electronic Devices for Microwave and Millimeter-Wave Power Applications," *Proc. IEEE*, **79**, pp. 598-620, 1991.

V. Cubic Boron Nitride Thin Film Growth

A. Introduction

Cubic boron nitride is a material with potential applications due to both its tribological and electronic properties. It is the hardest material other than diamond, and it is more stable than diamond at higher temperatures. It does not react with the ferrous metals, which makes it an ideal cutting tool material. For electronic applications, it is of interest because it is a wide band gap (E_g=6.4 eV) semiconductor with very high thermal conductivity; yet it also has the potential of being doped as both a p-type and n-type semiconductor. Boron nitride is similar to carbon in having three basic structures, a layered hexagonal structure (h-BN) corresponding to graphite, a cubic structure (c-BN) corresponding to diamond, and a rare hexagonal wurtzite structure (w-BN) which corresponds to Lonsdaleite. The layered hexagonal structure is typically referred to simply as hexagonal BN. There are also variations of these structures, including turbostratic BN (t-BN), which, like hexagonal BN, consists of layers, but in which the layers are randomly oriented to each other [1].

Bulk cubic boron nitride was first synthesized in 1956 using high pressure-high temperature methods [2]. In recent years, cubic boron nitride has been grown in thin film form, using both chemical vapor deposition (CVD) and physical vapor deposition (PVD) methods [3-7].

In this work we are studying the growth of cubic boron nitride thin films, and attempting to grow films which could be used for electronic applications. We have studied the evolution of the films as they grow, and found that the phase of the films changes during growth. On Si substrates an initial amorphous BN layer forms, followed by a hexagonal BN layer, followed by growth of the cubic phase. These results have been written up and submitted to the Journal of Materials Research. A preprint of this article is included as Section VI.

We are also studying how the films grow on various substrates. In addition to growing the films on Si substrates, we have grown them on both single crystal diamonds and on diamond thin films. We have also used the c-BN films grown on Si substrates as substrates for diamond growth.

B. Experimental Procedure

Film Growth

A UHV ion beam assisted deposition (IBAD) system is being used for film deposition. Samples are loaded through a load lock system. Base pressures in the chamber are typically $< 1\times10^{-9}$ Torr. Boron is deposited by evaporating boron metal using an electron beam evaporator. Simultaneously a Kaufman type ion gun is used to bombard the depositing boron with both nitrogen and argon ions. The films are deposited onto heated substrates. A

schematic of the setup is shown in Figure 1. The deposition rate of the boron, the energy and flux of the ions, the ratio of the argon to nitrogen, and the substrate temperature can all be measured, controlled, and varied. The boron is evaporated using a Thermionics HM2 electron gun with an electromagnetic beam sweep. The boron sits in a graphite crucible liner which is in a water cooled 10 cc crucible. It is deposited at a rate of from 0.25 to 1.0 Å/s. The deposition rate is monitored using a quartz crystal monitor.

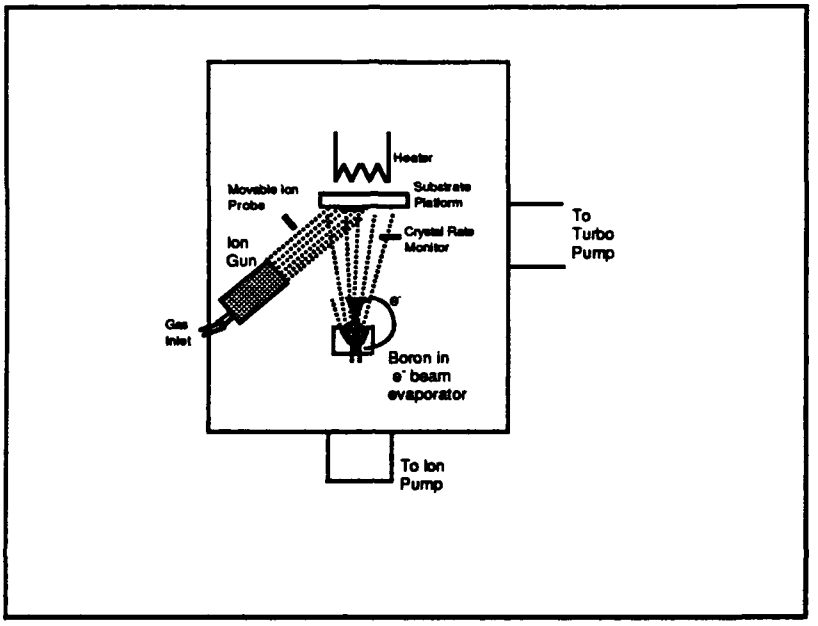

Figure 1. Schematic of deposition system.

The film is bombarded using an Ion Tech 3 cm Kaufman ion source. Bombardment is by nitrogen and argon ions in varied ratios, all at 500 eV. The flux of ions ranges from 0.05 to .30 mA/cm^2 and is measured using a negatively biased ion probe. The gas flow to the ion gun is 1.5 sccm for each of the two gases and is controlled using MKS mass flow controllers. Typical deposition pressures in the chamber are 1.0×10^{-4} Torr.

Substrates are heated from 300 to 700°C. The substrates used are 100 silicon wafers with high resistivity (25-45 W-cm) so as to be transparent for IR spectroscopy. Film thicknesses range from 100Å to 2000Å.

Film Characterization

FTIR. Fourier transform infrared spectroscopy (FTIR) has been found to be a convenient and reliable method for the purpose of determining whether a deposited film is cubic or hexagonal boron nitride. With FTIR analysis the cubic and hexagonal forms of boron nitride give distinct, independent peaks, due to the sp^3 and sp^2 bonds, respectively. Hexagonal boron

nitride has absorption peaks at 1367 cm^{-1} and at 783 cm^{-1} [8], while cubic boron nitride has a transverse optical mode absorption peak at 1075 cm^{-1} [9].

Transmission FTIR was carried out on an Analect Instruments model fx-6260 spectrometer. Transmission spectra were taken through the BN films and Si substrates. A spectra of an uncoated Si wafer was taken as a background scan, and the spectra of the coated wafer was ratioed against it. The Si wafers used as substrates were high resistivity wafers, >50 Ω cm, so as to transmit the IR radiation.

Reflectance FTIR was performed on films coated on substrates which are opaque to IR radiation, specifically Ni and Cu. This work was done on a Nicolet 620 FTIR with a Spectra Tech IR Plan optical microscope.

Electron microscopy. Structural characterization was accomplished by scanning electron microscopy (SEM) and transmission electron microscopy (TEM). SEM was performed in an Hitachi S-800 with a field emission gun. The samples were coated with a thin conductive layer of carbon to avoid charging effects. Carbon was deposited on a different area of the sample than that used for preparation of TEM samples. TEM was performed in a TOPCON EM-002B operated at 200 kV and a JEOL 4000EX operated at 400kV. On the JEOL microscope, high resolution images were recorded using a 1mr convergence semi-angle at Scherzer defocus (~ -47nm). Cross-sectional transmission electron microscopy (XTEM) samples were prepared using standard techniques [10].

XPS. X-ray photoelectron spectroscopy (XPS) was used to study the films. A Riber system, consisting of a Mac2 semi-dispersive electron energy analyzer and accessible by UHV transfer from the deposition chamber, was used. A Mg anode was used at 1.2 eV resolution for obtaining valence structure and 0.8 eV resolution for core level data.

Rutherford Backscattering. The stoichiometry of the films was measured using Rutherford backscattering (RBS), in which helium nuclei are used to bombard the film. By measuring the energy and angle of the backscattered nuclei, information about the film composition can be determined. RBS is particularly useful in that it gives a depth profile of the film, not only information about the surface layer.

C. Results

BN on single crystal diamond

Boron nitride was deposited on single crystal diamond. The diamond was natural diamond which had been cut and polished into substrates, obtained from Dubbledee company. Before loading, the diamonds were etched in a boiling H_2SO_4:HNO_3:$HClO_4$ solution in a ratio of 3:4:1 for 45 minutes to remove any graphitic phase. 1000 Å of BN was grown on the diamond, at substrate temperatures of 400° and 600°C. The FTIR patterns of the films are shown in Figure 2. A sharp c-BN peak is observed at ~1080 cm^{-1}. The h-BN peak is very

small. This spectra has a sharper c-BN peak, and a better c-BN to h-BN ratio than any films we had previously deposited on Si, and is as good or better than any that have appeared in the literature.

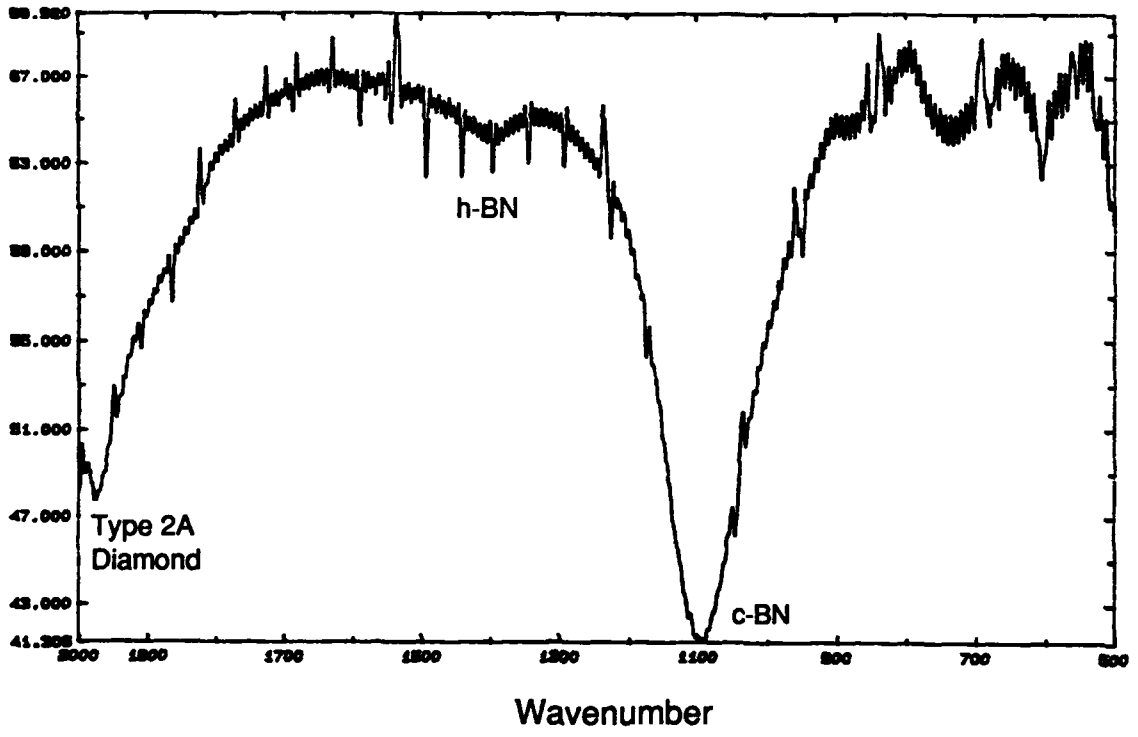

Figure 2. FTIR spectrum of BN film on single crystal diamond.

SEM of the sample deposited at 400°C showed some cracking of the film in spots. The film deposited at 600°C did not show any cracking or delamination. Films deposited at the same deposition conditions and the same thickness on Si are found to have major cracking and delamination of the BN film.

High resolution TEM (HRTEM) was performed on the samples, and the images are shown in Figs. 3 and 4. It can be seen on these two images that the same type of layered structure observed on BN grown on Si is present, if not as pronounced. On the 400° image the hexagonal and cubic regions appear more intermixed.

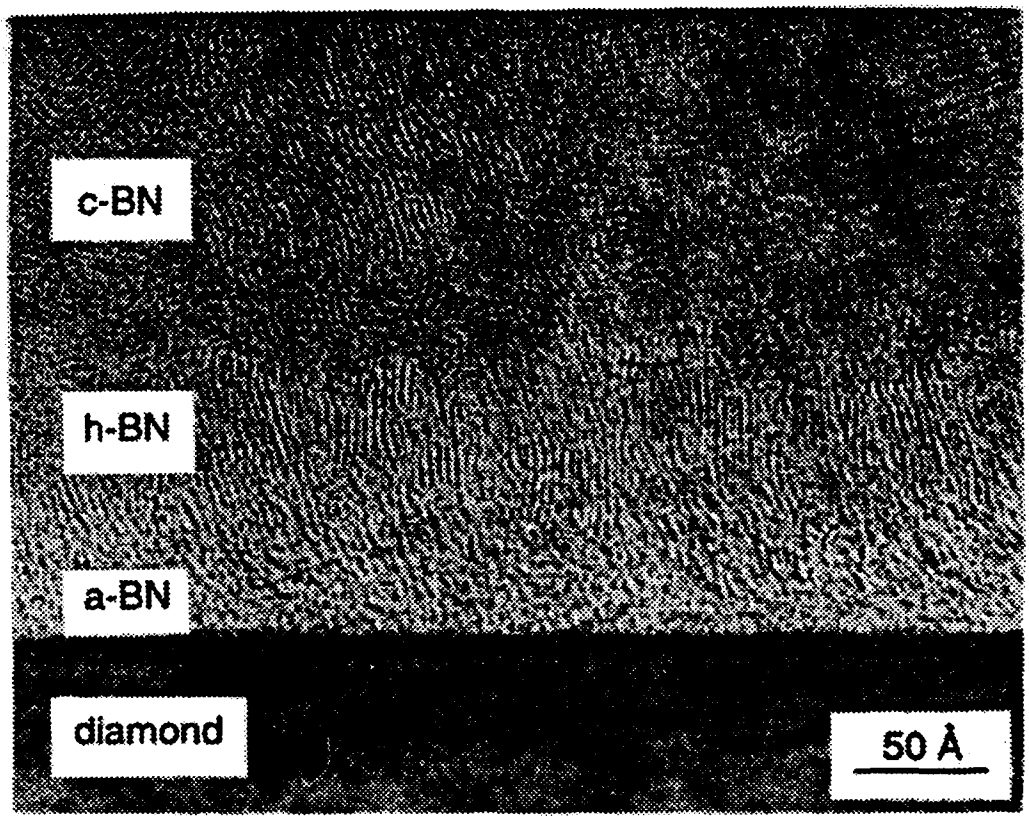

Figure 3. HRTEM of BN on diamond, grown at 400°C

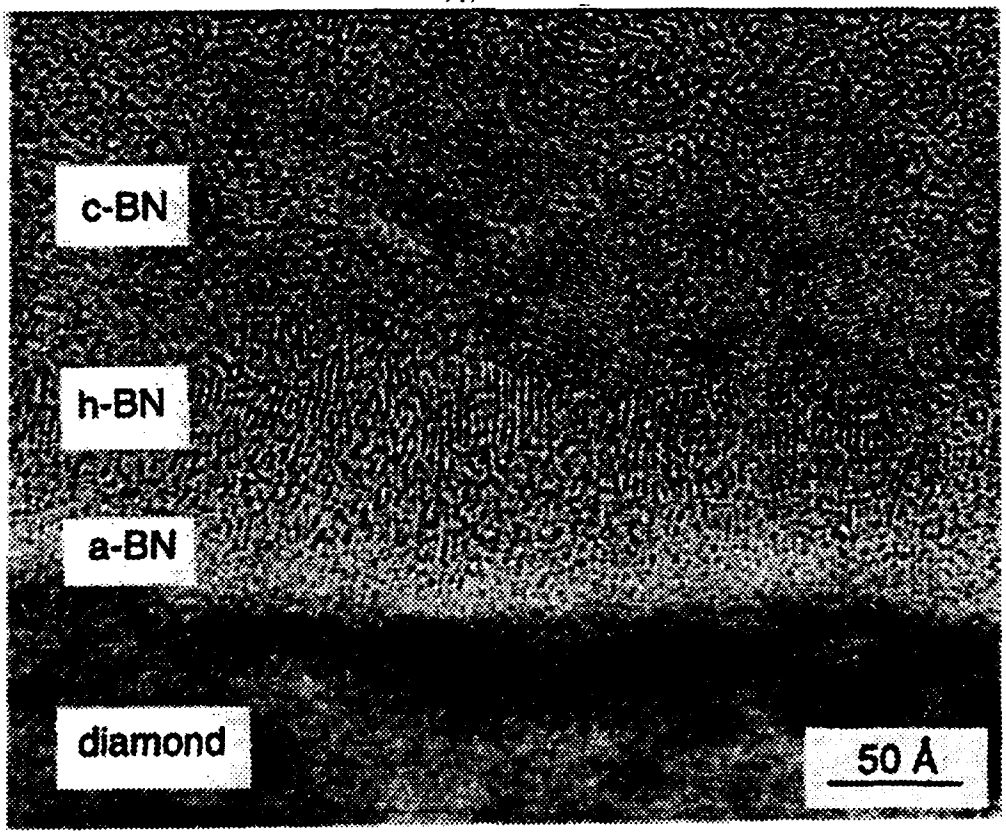

Figure 4. HRTEM of BN on diamond, deposited at 600°C

BN on diamond films

1000 Å of BN was grown on diamond thin films. The diamond films were grown on Si substrates using a microwave CVD process with 1% CH_4 and were 2-4μm thick. Before the c-BN deposition the substrates with the diamond films were etched in a boiling acid solution as described above.

HRTEM was performed on the films, however due to the roughness of the diamond surface a clear image could not be obtained. Therefore diamond films on silicon on which the diamond surface had been polished smooth were acquired and 1000 Å BN deposited on those. SEM of the films showed the presence of what appeared as black spots on the surface of the films. It is not yet clear what the source of the spots is, although they may be due to holes in the BN film brought about by the ion bombardment. HRTEM of these films will occur in the near future.

Raman spectroscopy was also performed on these films. The c-BN peak was not observed. This is not unexpected, as getting the raman peak generally requires more crystallinity than we have been able to achieve.

Diamond films on BN films

Diamond films were grown on BN films which had been deposited on Si substrates. The thickness of the BN films was 150Å. This was thick enough that the surface of the film would be cubic, but not thick enough for delamination to be a problem. The diamond was grown on these BN films using substrate biasing to help in nucleation of the diamond, as described in Ref. 11. Observation of the plasma during diamond growth showed the plasma to be an unusual color, which may indicate that the BN was being etched during the initial diamond growth, due to bombardment. SEM of the sample showed diamond to have formed on areas of the substrate. It is not clear whether the diamond growth occurred on the BN or on areas where BN had been etched off.

We are presently growing new diamond films on BN films without using the substrate biasing. This is being done on three different thicknesses of BN film: 20Å, 50 Å, and 150Å. These thicknesses correspond to the thicknesses at which the BN surface is amorphous, hexagonal, and cubic, respectively. These experiments may give information on how diamond nucleates on the different BN phases.

BN on Si

XPS. BN films were grown on Si and XPS was performed on them. Films were 20 Å and 100 Å thick. Other than thickness, deposition conditions were identical. The XPS could get data on the top 50 Å of the film, this allowed us to compare the Si-BN interface with the BN material in the film at 50-100Å. It is seen in Fig. 5 that at the interface there are both Si-Si

(99 eV) and Si-N bonds (101 eV) present. This indicates that there is not an abrupt transition from the Si substrate to the BN film, but that the nitrogen ion bombardment causes the formation of an interfacial silicon nitride (Si_3N_4) layer.

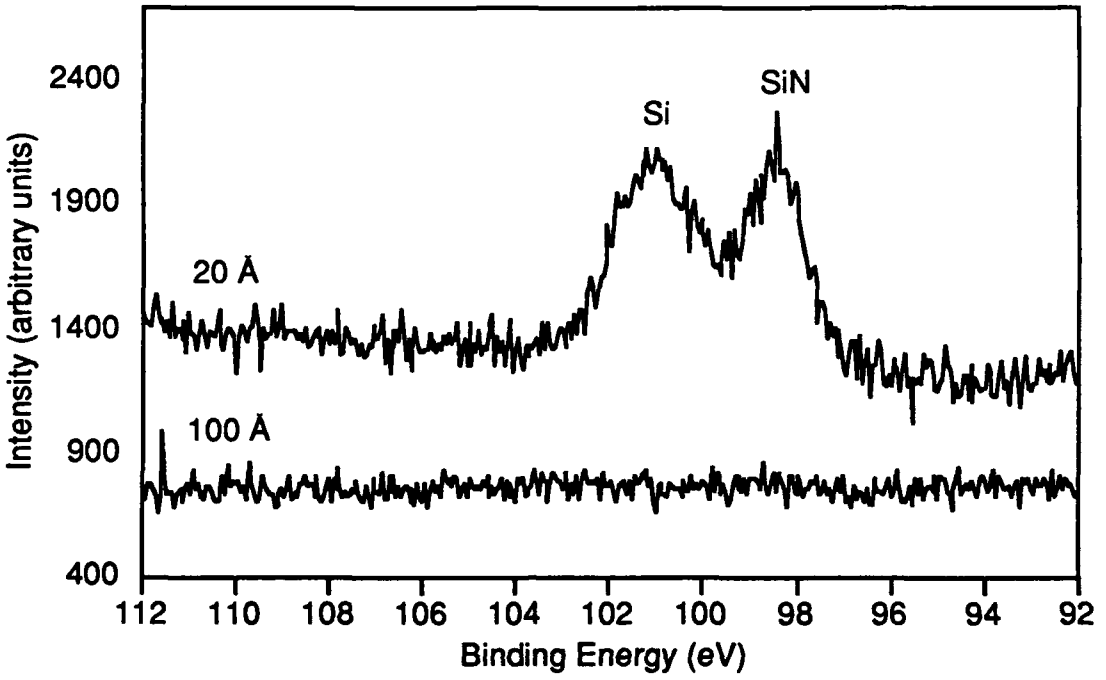

Figure 5. XPS spectra showing Si peaks on 20Å and 100Å thick films.

In Figure 6 the boron XPS peaks for the two films are shown. It is seen that on the 100 Å film the peak due to BN is present. On the 20 Å film there is the BN peak, but also a shoulder that appears to be due to the elemental B peak. This would indicate that near the interface there is both N bonded and B bonded B present.

Figure 7 shows the XPS peaks for Ar. It is seen that there is not much difference between the film at 20 Å and at 100Å. Both contain a detectable amount of Ar.

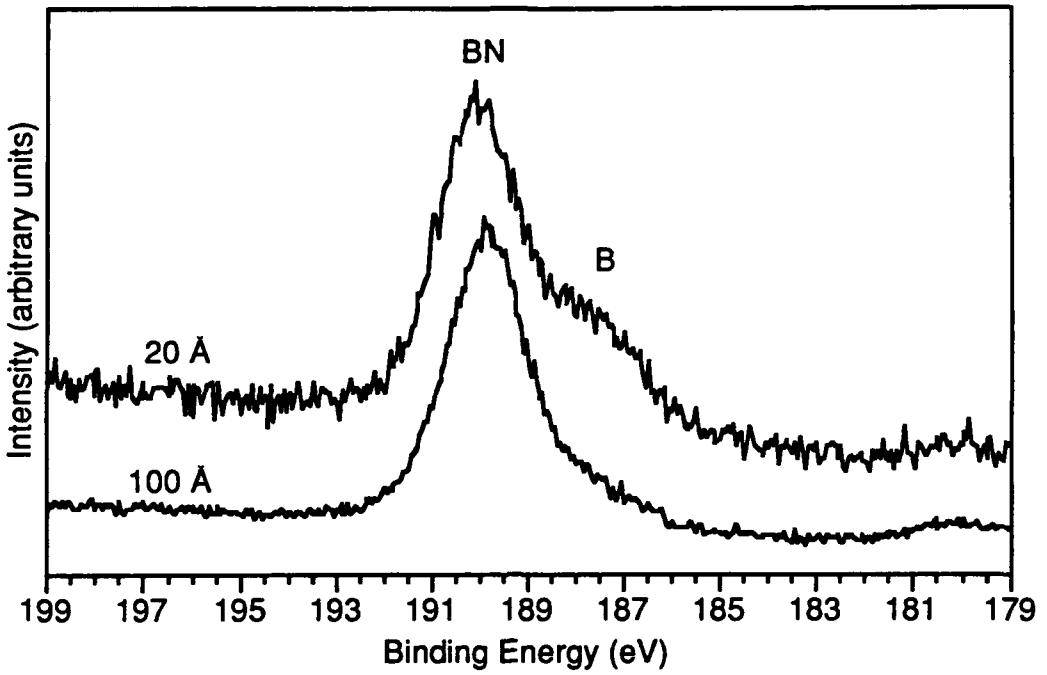

Figure 6. XPS spectra showing B peaks on 20Å and 100Å thick films.

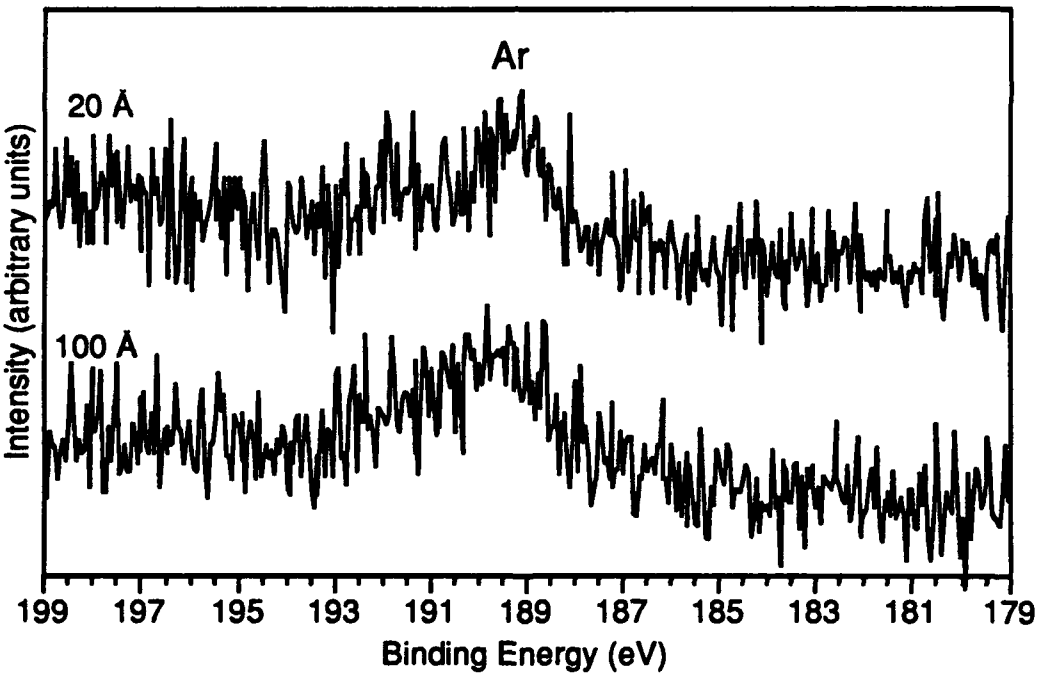

Figure 7. XPS spectra showing Ar peak on 20Å and 100Å thick films.

RBS. For RBS it is preferred that the substrate material have a lower atomic number than the film material. Otherwise the spectrum of the substrate will overlap that of the film material, making the film spectra difficult to read. Therefore the film for RBS was deposited on a Be

substrate. Results are shown in Figure 8. RBS is more sensitive to materials of higher atomic numbers, due to their larger nuclear cross sections. Therefore, the size of the peaks of the materials at various channel numbers does not directly show their actual concentration. Computer modeling of the spectra showed that in addition to the expected Be, B, and N, there is also O at the Be surface, and Ar, Fe, and Hf present in the film. The modeling indicates that the O peak is due to a BeO layer between the Be substrate and BN film, and that the atomic percentage of Ar was ~1.5%, of Fe ~0.2%, and of Hf ~0.05%. The source of the Ar would be the Ar ion bombardment during growth, the Fe is probably due to the ion beam bombarding the stainless steel shutter above the substrates, sputtering Fe onto the film. The Hf may be due to the deposition system also being used for Hf film deposition, and previously deposited Hf from the substrate block being sputtered.

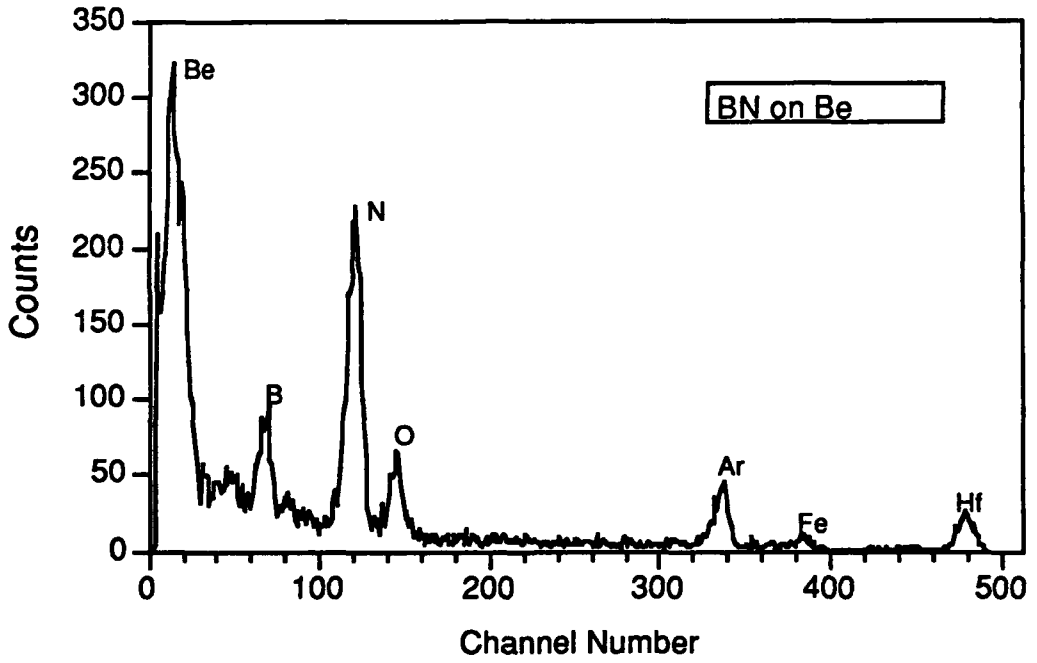

Figure 8. RBS spectra of BN film on Be substrate.

Growth of initial boron layer. The XPS analysis showed that an initial Si_3N_4 layer was forming at the Si surface. It was thought that the formation of this layer may be inhibiting the epitaxial growth of c-BN. Therefore attempts were made to deposit an initial boron layer before starting the ion bombardment. Boron layers of 20 Å, 50 Å, and 100 Å were deposited under conditions found to lead to cubic growth. FTIR examination of the films showed that all still had a significant h-BN component.

Other substrates. Ni and Cu have lattice spacing very close to that of c-BN. Therefore it was thought that they may be better substrates for c-BN than Si which has a lattice mismatch of 34%. Reflectance FTIR was performed on these films.

Films were grown under conditions which had been found to give c-BN films on Si. Films grown on the Ni substrate were found to be mixed h-BN and c-BN (Figure 9); films grown on Cu were h-BN with no evidence of the presence of c-BN (Fig. 10).

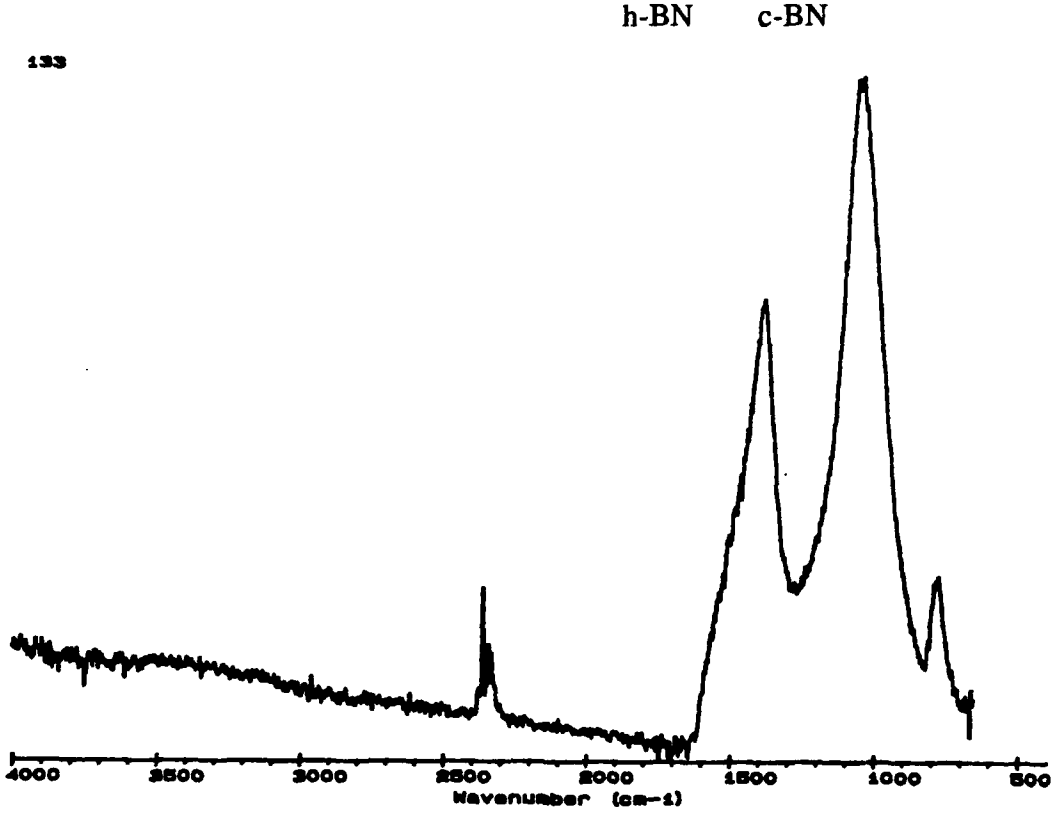

Figure 9. Reflectance FTIR of BN film on Ni substrate.

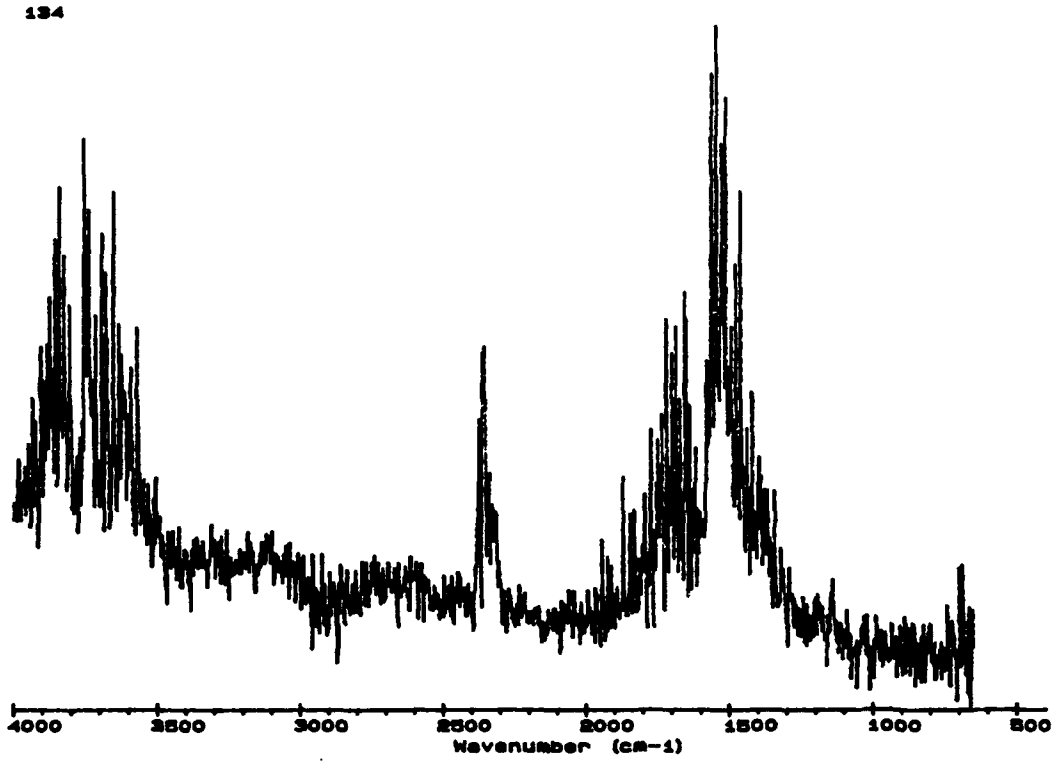

Figure 10. Reflectance FTIR of BN film on Cu substrate.

Patterned substrates

Selected area deposition was performed on patterned Si substrates. These consisted of Si wafers which had been coated with an SiO_2 layer. Holes were etched into the SiO_2, to expose the Si in regions of varying diameters. Examination by SEM showed that good adhesion of the BN film on the Si occurred within the etched holes. The material deposited on the SiO_2 around the holes, had poor adhesion.

D. Discussion

The results shown in the paper in Appendix A demonstrate that cubic boron nitride grows on Si with an initial amorphous layer, followed by a hexagonal layer, followed by the growth of cubic material. The fact that the phase changes at some point in the film growth to the metastable cubic phase indicates that at the non-equilibrium deposition conditions used, cubic is the stable phase. This leads to the question of why the film growth is not cubic, but is initially amorphous, and whether it is at all possible to grow epitaxial c-BN. The lack of any repeatable examples of epitaxial c-BN in the literature raises the same question. It was initially thought that the problem was due to the poor lattice mismatch between Si and c-BN. However the results obtained using other substrates with excellent lattice matching showed this not to be the case. It has previously been predicted that c-BN can grow epitaxially on diamond [12]. Yet a

layered structure similar to that observed on Si was also seen on films grown on diamond substrates. Depositions on Cu (with an exact lattice match to c-BN) and on Ni also gave mixed phase films. The fact that depositing an initial layer of boron did not improve the films also indicates that the Si/BN interface itself may not be the problem.

The results presented in Appendix A showed that there is not a sharp change at the interface from Si to cubic BN. The XPS results that there is both Si_3N_4 and elemental B (B bonded to other B, not to N) at the interface show that not only is there not a sharp transition to cubic phase BN, but that there is not a sharp transition from Si to BN of any phase. For epitaxial c-BN a sharp Si to BN transition would be the first requirement. The ion bombardment itself, while apparently necessary to grow c-BN [13] may in itself be preventing the growth of epitaxial c-BN by forming a Si_3N_4 layer.

Recent work [14] suggests that c-BN forms due to the buildup of stress in the growing films. That study suggests that the onset of the cubic phase will not be initiated until the compressive stress is high enough, which will not occur until a certain film thickness is reached. Our results appear to confirm this.

The actual mechanism causing the stress in the film is not clear. It may be densification due to the ion bombardment. Densification and associated stress has been previously observed in ion bombarded films [15]. The densification occurs through the collapse of the void structure found in non-bombarded films. The stress may also be due to the presence of interstitials in the film. In the case of the c-BN films, the relatively high concentration of Ar (1.5 at.%) as shown by RBS and XPS suggests that the compressive stress may be caused by interstitial Ar atoms.

E. Conclusions

HRTEM and FTIR studies have revealed that BN growth on Si(100) substrates occurs as a single sequence of thin amorphous, hexagonal and cubic layers. The c-BN is single phase and does not undergo further transformation to a thickness of ≈1000Å.

c-BN did not grow epitaxially on any substrate. This may be due to the need for a certain level of compressive stress in the films before the initiation of the cubic phase. This compressive stress would not be reached until the film has grown to a certain thickness (50-100Å). The cause of the compressive stress may be interstitial Ar in the film.

F. Future Research Plans/Goals

Work is continuing on depositing BN on diamond films. We are obtaining a number of oriented 100 diamond films, to use as substrates. This will allow the growth of films at a wider range of deposition conditions then we were able to do on single crystal diamonds. The effect of both substrate temperature and bombardment level will be examined.

BN films on Si have been deposited at different thicknesses which will give different BN phases at the film surface. Diamond films are being grown on these and the effect of the different BN phases on diamond nucleation is being studied.

We are in the process of doing a systematic study of the effect of substrate temperature on the growth of BN on Si. Films are being characterized by FTIR and HRTEM.

Auger electron spectroscopy will be used to examine the first 200 Å of a BN film, to see how the composition varies with thickness. This may give some insight into how the phase evolution of the film develops.

The effect of post-deposition annealing will be studied. It will be seen if this has any effect on the structure of the films.

G. References

1. J. Thomas, Jr., N. E. Weston, and T. E. O'Conner, J. Am. Chem. Soc. **84**, 4619 (1963).
2. R. H. Wentorf, Jr., J. Chem. Phys. **26**, 956 (1957).
3. F. Shimokawa, H. Kuwano, and K. Nagai, Proc. 9th Symp. on ISIAT 85 Tokyo (1985).
4. K. Inagawa, K. Watanabe, H. Ohsone, K. Saitoh, and A. Itoh, J. Vac. Sci. Technol. **A5**, 2696 (1987).
5. Y. Andoh, K. Ogata, and E. Kamijo, Nucl. Instrum. Methods Phys. Res. **B33**, 678 (1988).
6. M. Murakawa and S. Watanabe, Surf. Coat. Technol. **43/44**, 128 (1990).
7. H. Saitoh, T. Hirose, H. Matsui, Y. Hirotsu, and Y. Ichinose, Surf. Coat. Technol. **39/40**, 265 (1989).
8. R. Geick and C. H. Perry, Phys. Rev. **146**, 543 (1966).
9. P. J. Gielisse, S. S. Mitra, J. N. Plendl, R. D. Griffis, L. C. Mansur, R. Marshall, and E. A. Pascoe, Phys. Rev. **155**, 1039 (1967).
10. C. H. Carter, Jr., J. A. Edmond, J. W. Palmour, J. Ryu, H. J. Kim and R. F. Davis in *Microscopic Identification of Electronic Defects in Semiconductors*, edited by N. M. Johnson, S. G. Bishop, and G. Watkins (Mater. Res. Soc. Proc., **46**, Pittsburgh, PA 1985) pp. 593 -598.
11. B. R. Stoner, G.-H. M. Ma, S. D. Wolter, and J. T. Glass, Phys. Rev. B, **45**, 11067 (1992).
12. M. W. H. Braun, H. S. Kong, J. T. Glass, and R. F. Davis, J. Appl. Phys. **69**, 2679 (1991).
13. D. J. Kester and R. Messier, J. Appl. Phys., **72**, 504 (1992)
14. D. R. McKenzie, talk given at the 1992 American Vacuum Society annual meeting, Chicago, IL, November 1992.
15. R. A. Roy and D. S. Yee, in *Handbook of Ion Beam Processing Technology*, edited by J. J. Cuomo, S. M. Rossnagel, and H. R. Kaufman, (Noyes, Park Ridge, NJ, 1989).

VI. Phase Evolution in Boron Nitride Thin Films*

D. J. Kester, K. S. Ailey, K. L. More, and R. F. Davis

Department of Materials Science and Engineering, North Carolina State University, Raleigh, NC 27695

Boron nitride (BN) thin films were deposited on monocrystalline Si (100) wafers using electron beam evaporation of boron with simultaneous bombardment by nitrogen and argon ions. The effect of film thickness on the phase of BN was investigated using Fourier transform infrared (FTIR) spectroscopy and high resolution transmission electron microscopy (HRTEM). These techniques revealed the consecutive deposition of an initial 20Å thick layer of amorphous BN, 20-50Å of hexagonal BN having a layered structure, and a final layer of the cubic phase. The growth of the non-cubic layers are believed to act as a residual stress relief mechanism and/or to form surface and interface relationships which become favorable for the nucleation of the cubic phase. The presence of the amorphous and hexagonal regions may also explain why there have been no reports of the growth of 100% cubic boron nitride on Si.

*Submitted for publication to the Journal of Materials Research

Boron nitride is similar to carbon in having three crystalline structures:[1] a layered hexagonal structure (*h*-BN) corresponding to graphite, the cubic structure (*c*-BN) analogous to diamond, and a rare hexagonal wurtzite structure (*w*-BN) corresponding to Lonsdaleite. The last two phases are metastable under normal environmental conditions. An amorphous phase (*a*-BN) is also common in films and coatings.

The extreme mechanical and thermal properties of *c*-BN make it useful for wear-resistant tools for the machining of steels, for corrosion resistant and electrically insulating parts, and for heat sinks for electronic devices. It has also recently been shown that bulk single crystals of this wide bandgap (E_g≈6.4 eV) semiconductor can be doped with both n- and p-type impurities and that light emitting p-n junctions can be produced [2]. This phase combined with other BN phases, has also been achieved in thin film form via physical vapor deposition [3-5] and chemical vapor deposition [6] methods.

Most researchers growing BN films use FTIR spectroscopy for phase identification. The cubic phase of BN has a distinct absorption peak at about 1080 cm^{-1}. The hexagonal, turbostratic (disordered hexagonal), and amorphous phases have primary and secondary absorption peaks at 1370 and 780 cm^{-1}, respectively. Thus, these non-cubic phases cannot be distinguished using FTIR. A commonly reported feature of these spectra obtained from analyses of the total thickness of the films wherein the presence of *c*-BN is apparent is the indication of various amounts of the hexagonal and/or amorphous phases (see, e.g., Refs. 4, 5). The FTIR spectra of the films obtained in the present research showed similar results. However, the unusual evolution of these phases has been determined by HRTEM and has been correlated with the FTIR results.

The Si (100) substrates used in the present study received a standard RCA cleaning [7] which included a 5 min. dip in 10% HF as the final step. This left the surface H-terminated and reduced the rate of reaction of this surface with H_2O and O_2 in the atmosphere. The substrates were subsequently transferred to the deposition chamber and heated to 400°C under UHV conditions. Base and deposition pressures were typically $<10^{-9}$ Torr and 10^{-4} Torr, respectively. The growth method involved the electron beam evaporation of B sufficient to achieve a deposition rate of 0.25 Å/s, as measured via a quartz crystal rate monitor. The growing films were simultaneously bombarded with a 0.12 mA/cm^2 ion flux (measured using a biased probe) of 500 eV nitrogen and argon ions produced in a Kaufman source using a 50:50 gas flow ratio of Ar/N_2. A shutter was used to cover the substrate prior to film deposition while the boron evaporation and ion bombardment were brought to correct levels for deposition and allowed to stabilize. Conditions during each deposition were maintained constant. The total film thickness ranged from 125-500Å.

FTIR was performed using an Analect Instruments model fx-6260 spectrometer. Transmission spectra were taken through the BN films and Si substrates. A spectra of an

uncoated Si wafer was taken as a background scan, and the spectra of the coated wafer was ratioed against it. The spectra for films deposited under identical conditions except for growth time are shown in Fig. 1. Peak heights were maximized on each of the spectra, thus only the ratio of peak heights within a single spectra are meaningful; absolute peak heights on different spectra cannot be compared. The relative amount(s) of non-cubic phase(s) was high for very thin films (<200Å). As the deposition time and resulting thickness increased, the relative percentage of the cubic phase increased. This indicated that the ratio of the concentration of the *c*-BN phase to that of the *a*-BN and *h*-BN phases increased as a function of film thickness rather than being constant regardless of deposition time.

To test this hypothesis, structural characterization of the films as a function of thickness was performed via HRTEM using a TOPCON EM-002B microscope operated at 200kV. Cross-sectional samples of the BN films were prepared using standard techniques [8]. The HRTEM images, an example of which is shown in Fig. 2, supported the above hypothesis in that they revealed that three distinct regions had deposited in the following sequence: an initial layer of about 20Å of *a*-BN at the Si (100) interface, a layer of 20-50 Å of *h*-BN, and a top layer of polycrystalline, random oriented cubic material. The hexagonal layers grew perpendicular to the Si (100) surface. An optical diffraction pattern was obtained by performing a Fast Fourier Transform on the HRTEM image to obtain the diffraction information shown in Fig. 3. The lattice spacings for the top layer matched that of *c*-BN, while those within the middle layer matched that of *h*-BN.

As noted above, all reported transmission FTIR spectra obtained from analyses of the total thickness of BN films have indicated the presence of some non-cubic phase. Explanations for this phenomenon include: (1) the occurrence of the non-cubic phases(s) on the grain boundaries within the *c*-BN matrix; (2) separate *h*-BN or *a*-BN micro-regions distributed throughout the films; and (3) a layered sequence of these various phases. Microstructures produced by combinations of these three factors may also exist in the films. The results of the present research indicate that sequential layers of *a*-BN and *h*-BN are the sources of the non-cubic phases. The HRTEM image shows that once the growth of the cubic phase is initiated, this layer is single phase. More specifically, even non-cubic grain boundary regions were not observed. Upon nucleation, the cubic phase grows without further transformation, at least to the maximum layer thickness thus far deposited (≈1000Å).

The exact reason(s) for the occurrence and layer sequence within the microstructure shown in Fig. 2 is (are) not known. Previous work on BN film growth [9] has shown that, for a given substrate temperature, the deposition of a particular phase is a function of momentum transferred into the film by the ion bombardment. The deposition conditions used in this study were those that previously resulted in the growth of films containing substantial concentrations of *c*-BN. However, nucleation of this phase is obviously not automatic. The amorphous

phase may occur initially as a transition zone of reduced residual stress relative to that which would develop during *epitaxial* growth of *c*-BN (or *h*-BN) on Si(100) due to the large mismatch in lattice parameter (≈33.4 % for *c*-BN). This constraint may be joined or surmounted by the constraint of surface energy. It may be impossible for *c*-BN (or even h-BN) to nucleate and grow *epitaxially* on Si(100) due to the much larger surface energy of the BN crystalline phases.

The transformation of the *a*-BN to the *h*-BN phase is not surprising from the viewpoint of equilibrium thermodynamics under standard conditions. However, as noted above, the experimental parameters favored the nucleation of *c*-BN. The explanation for the nucleation of *h*-BN may be found in the atomic structure of the *a*-BN. X-ray radial distribution curves normally show that stoichiometric amorphous phases are similar in atomic arrangement to their crystalline analogs, especially among nearest neighbors and occasionally to even greater spheres of coordination. The essentially indistinguishable IR spectra between *a*-BN and *h*-BN also indicate similar atomic arrangements in these two phases which may explain the subsequent nucleation of this phase. The reason for the preferred orientation of the basal plane of the *h*-BN perpendicular to the Si(100) surface is not known, though it may also be related to the atomic structure of the *a*-BN surface.

A three dimensional phase transformation only at the growing surface of a thin film phase normally considered to be the equilibrium structure (*h*-BN) to one which is metastable (*c*-BN) is truly an anomaly even under highly nonequilibrium conditions. The experimental conditions coupled with the presence of the high surface energy edges of the *h*-BN which acted as the substrates are believed to be the reasons for this unusual transformation. If this is the case, it would be analogous to the recent findings regarding nucleation of diamond on non-diamond substrates. Williams [10] has investigated personally and via review of the literature the sequence of deposition events leading to the onset of diamond nucleation on carbide- and noncarbide-forming substrates. In all documented cases, the deposition of a particulate amorphous and/or graphitic phase preceded the nucleation of diamond. Davis has argued [11] that the high energy edges of appropriately oriented graphite or other C particles are the likely sites for the onset of diamond nucleation (this scenario may also explain the considerable effectiveness of scratched substrates in that the scratches act to orient the C particles such that diamond nucleation is favored). The research of Angus and his colleagues [12, 13] concerned with the nucleation and growth of diamond on various orientations of pyrolytic graphite support this hypothesis. In this regard, recent research by the present authors involving the deposition and HRTEM of BN films on (100) single crystal diamond substrates under the same conditions noted above resulted in the initial deposition of a very thin *a*-BN layer and a subsequent layer containing a mixture of primarily *c*-BN and a small amount of *h*-BN. The details of this study will be reported in the near future.

Finally, a close examination of Fig. 2 reveals an uneven *h*-BN/*c*-BN interface but a very smooth *c*-BN surface. This indicates that (1) the initial nucleation of the c-BN did not occur simultaneously across the *h*-BN surface and (2) the deposition rate of these two phases is essentially the same. These results also show that *c*-BN does not form due to the elimination of the *h*-BN phase by the ion beam. The HRTEM results clearly show that the *h*-BN phase forms under the same conditions used to deposit *c*-BN. To date, it has not been possible to determine the orientation relationship between the *h*-BN and the *c*-BN phases at the site of nucleation.

In summary, HRTEM and FTIR studies have revealed that BN growth on Si(100) substrates occurs as a single sequence of thin amorphous, hexagonal and cubic layers. The *c*-BN is single phase and does not undergo further transformation to a thickness of ≈1000Å. The non-cubic layers are believed to occur initially to form relatively relaxed transition zones and/or to achieve a surface and interface energy relationship which eventually becomes favorable to the nucleation of the *c*-BN. The preferred orientation of the *h*-BN layers and the exposure of the high surface energy edges of this phase are believed to act in tandem with the highly non-equilibrium growth conditions to achieve the deposition of the *c*-BN.

Acknowledgments

The authors express their appreciation to the Electronic Materials Center of Kobe Steel, USA and the Strategic Defense Initiative through the Office of Naval Research and via the contract #N00014–92–J-1720 for support of this research and to Professor J. Angus of Case Western Reserve University for the information regarding the deposition of diamond on pyrolytic graphite and for giving us a preprint of the paper describing this research. A portion of the electron microscopy was supported as part of the Ceramic Technology for Advanced Heat Engines Program of the Advanced Materials Development Program and partially performed in the HTML User Facility, both sponsored by the U. S. Department of Energy, Assistant Secretary for Conservation and Renewable Energy, Office of Transportation Technologies, under contract DE AC0584ORO21400 managed by Martin Marietta Energy Systems, Inc.

References

[1] L. Vel, G. Demazeau and J. Etourneau, Mater. Sci. and Eng. **B10**, 149 (1991).

[2] O. Mishima, K. Era, J. Tanaka, and S. Yamaoka, Appl. Phys. Lett., **53**, 962 (1988).

[3] K. Inagawa, K. Watanabe, H. Ohsone, K. Saitoh, and A. Itoh, J. Vac. Sci. Technol. **A5**, 2696 (1987).

[4] Y. Osaka, M. Okamoto, and Y. Utsumi, Mater. Res. Soc. Symp. Proc., **223**, 81 (1991).

[5] N. Tanabe, T. Hayashi, and M. Iwaki, Diamond Relat. Mater., 1, 151 (1992).

[6] H. Saitoh, T. Hirose, H. Matsui, Y. Hirotsu, and Y. Ichinose, Surf. Coat. Technol. **39/40**, 265 (1989).

[7] W. Kern and D. A. Puo-tinen, RCA Rev. **31**, 187 (1970).

[8] C. H. Carter, Jr., J. A. Edmond, J. W. Palmour, J. Ryu, H. J. Kim and R. F. Davis in *Microscopic Identification of Electronic Defects in Semiconductors*, edited by N. M. Johnson, S. G. Bishop, and G. Watkins (Mater. Res. Soc. Proc., **46**, Pittsburgh, PA 1985) pp. 593 -598.

[9] D. J. Kester and R. Messier, J. Appl. Phys., **72**, 504 (1992)

[10] B. E. Williams, Ph. D. Dissertation, North Carolina State University, 1992

[11] R. F. Davis, Presentation at the 1991 Gordon Conference on Inorganic Thin Films.

[12] J. Angus (private communication).

[13] Z. Li, L. Wang, T. Suzuki, P. Pirouz and J. C. Angus, in press.

FIGURES

1. FTIR spectra of BN films of various thicknesses all deposited on Si (100) substrates under the following conditions: Boron deposition rate: 0.25 Å/s; ion energy: 500 eV; ion flux: 0.12 mA/cm^2; ion bombardment by 50:50 Ar:N_2; substrate temperature: 400°C.
2. Cross-sectional HRTEM image of BN film showing Si substrate and regions of amorphous BN (a-BN), hexagonal BN (h-BN), and cubic BN (c-BN).
3. Optical diffraction pattern from the HRTEM image of Fig. 2. (a) From the region labeled as h-BN. (b) From the region labeled as c-BN.

Figure 1

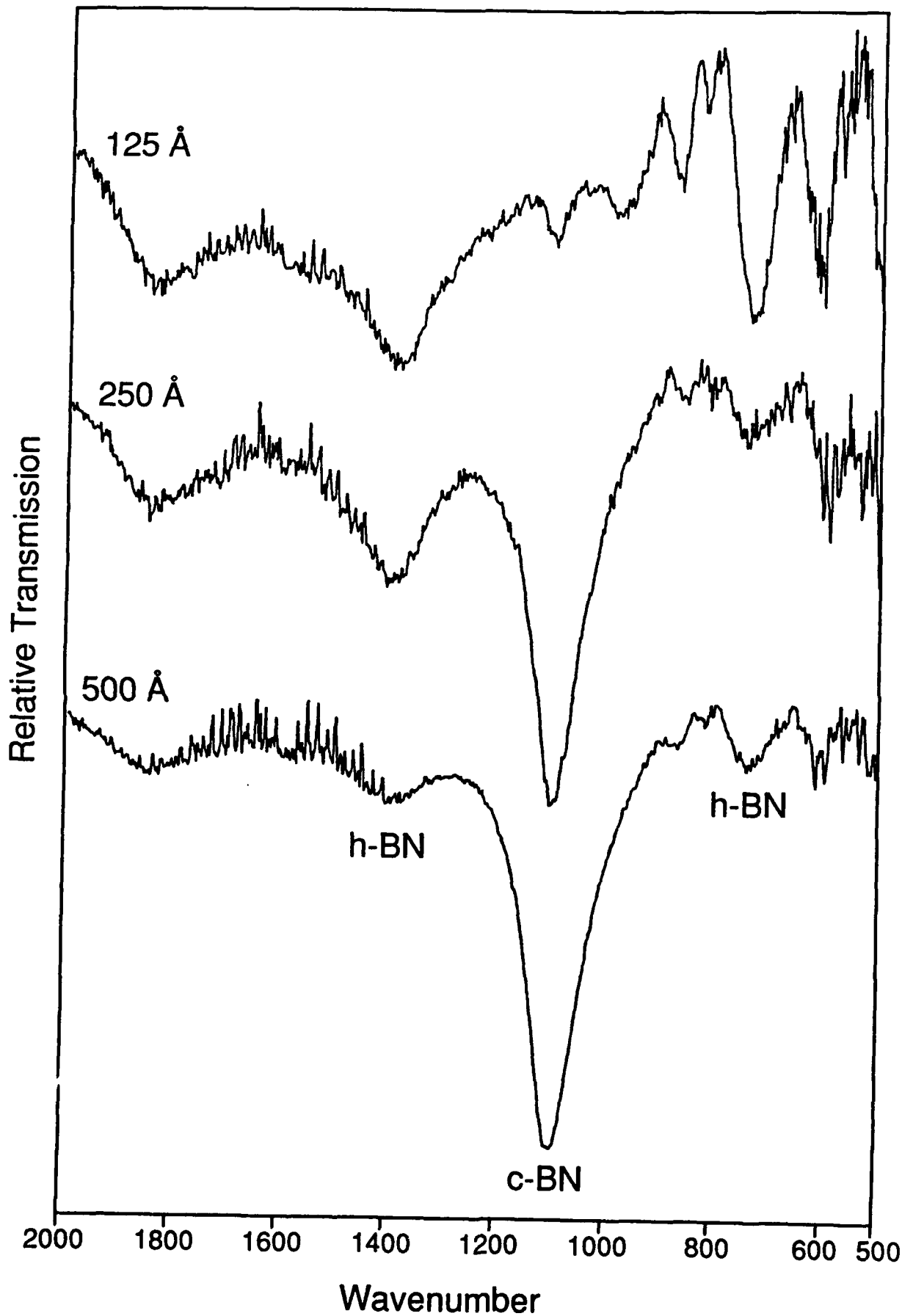
125 Å
250 Å
500 Å
h-BN
h-BN
c-BN
Relative Transmission
2000
1800
1600
1400
1200
1000
800
600
500
Wavenumber

Figure 2

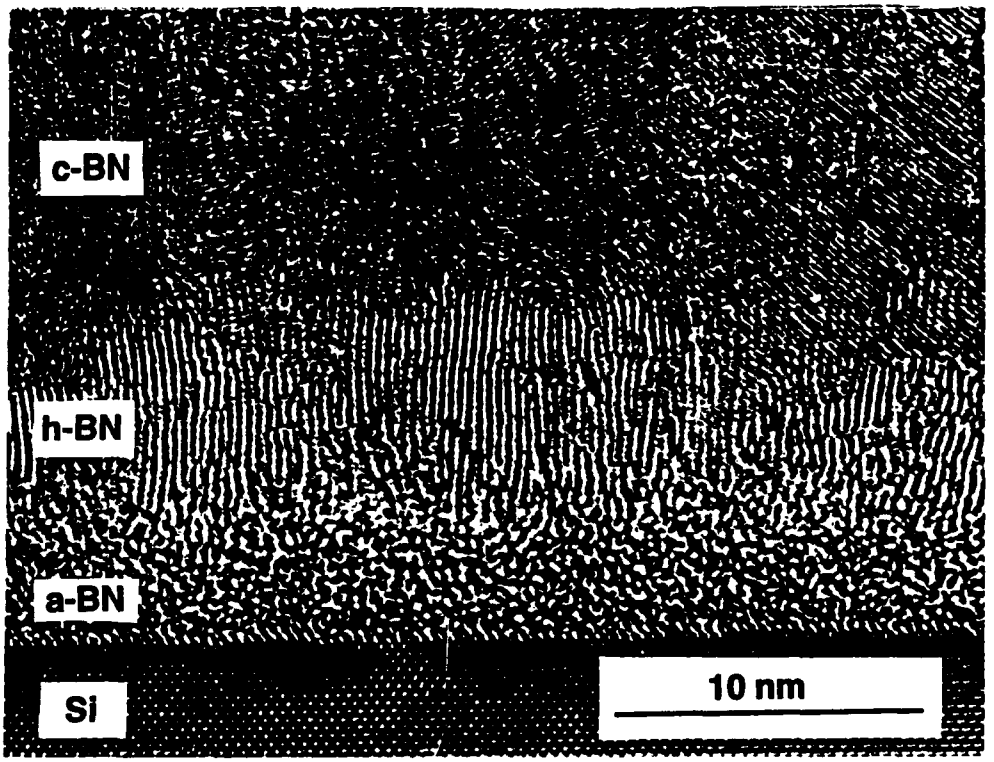

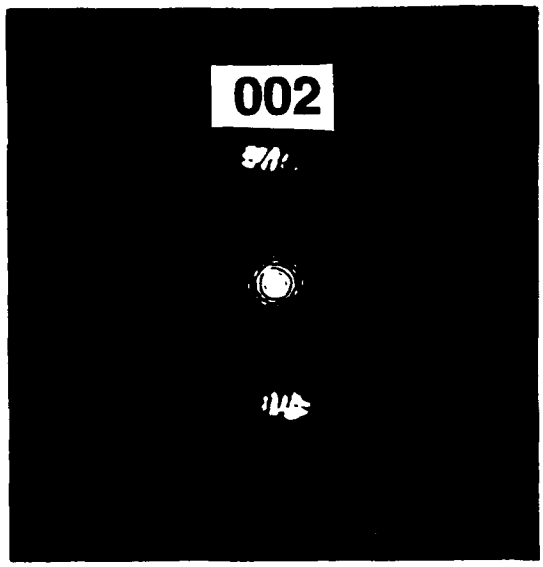

Figure 3a

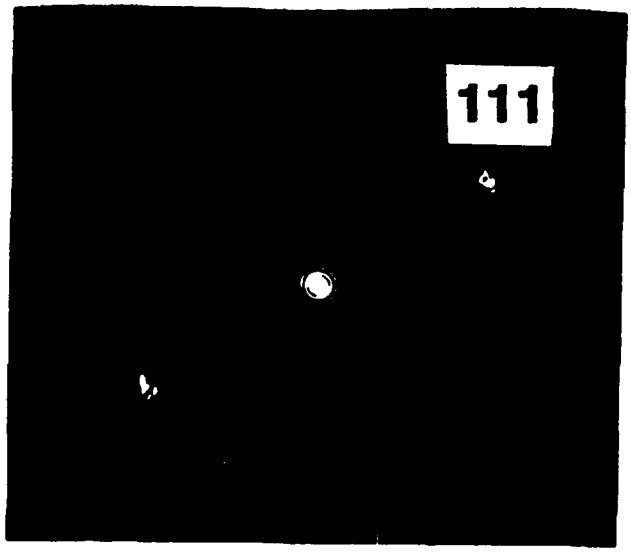

Figure 3b

VII. Distribution List

Mr. Max Yoder
Office of Naval Research
Electronics Program–Code 1114
800 North Quincy Street
Arlington, VA 22217

Office of Naval Research
Resident Representative
The Ohio State Univ. Research Center
1960 Kenny Road
Columbus, OH 43210-1063

Director
Naval Research Laboratory
Attention: Code 2627
Washington, DC 20314

Defense Technical Information Center
Building 5
Cameron Station
Alexandria, VA 22314

Robert J. Markunas
Research Triangle Institute
Post Office Box 12194
Research Triangle Park, NC 27709-2194

Dr. Ron Rudder
Research Triangle Institute
P. O. Box 12194
Research Triangle Park, NC 27709-2194

Howard Schmidt and Mark Hammond
Schmidt Instruments
2476 Bolsover, Suite 234
Houston, TX 77004

Prof. Karl Spear
Pennsylvania State University
201 Steidle
University Park, PA 16802

Michael W. Geis
Lincoln Laboratories
244 Wood Street
P. O. Box 73
Lexington, MA 02173

Professor R. F. Davis
Materials Science and Engineering
Box 7907
North Carolina State University
Raleigh, NC 27695-7907

Professor R. J. Nemanich
Department of Physics
Box 8202
North Carolina State University
Raleigh, NC 27695-8202

Professor R. J. Trew
Electrical and Computer Engineering
Box 7911
North Carolina State University
Raleigh, NC 27695-7911

Professor John C. Angus
Chemical Engineering
Case Western Reserve University
Cleveland, OH 44106

Dr. Andrzej Badzian
271 Materials Research Laboratory
The Pennslyvania State University
University Park, PA 16802

Dr. H. Liu
Emcore Corp.
35 Elizabeth Avenue
Somerset, NJ 08873

Prof. Karen Gleason
Chemical Engineering, Rm. 66-462
M. I. T.
Cambridge, MA 02134

Prof. Jerry Whitten
Chemistry
Box 8201
N. C. State University
Raleigh, NC 27695-8201

Dr. Ray Thomas
Research Triangle Institute
Box 12194
Research Triangle Park, NC 27709-2194

Allen R. Kirkpatrick
Epion Corp.
4R Alfred Circle
Bedford, MA 01730

Robert C. Linares
Linares Management Assoc., Inc.
P. O. Box 336
Sherborn, MA 01770

Dr. Martin Kordesch
Physics
Clippinger Research Laboratories
Ohio University
Athens, OH 45701-2979

Prof. Charter Stinespring
Chemical Engineering, Box 6101
West Virginia University
Morgantown, WV 26506

Robert Hauge
Chemistry
Rice University
Houston, TX 77251

Dr. John Margrave
HARC
4800 Research Forest Drive
The Woodlands, TX 77381

Dr. John Posthill
Research Triangle Institute
P. O. Box 12194
Research Triangle Park, NC 27709-2194

Dr. James Butler
NRL Code 6174
Washington, DC 20375

Dr. Andrew Freedman
Aerodyne Research, Inc.
45 Manning Road
Billerica, MA 01821

Prof. Michael Frenklach
Penn State University
202 Academic Projects Bldg.
University Park, PA 16802

Prof. Jeffrey T. Glass
Materials Science & Engr.
Box 7907
North Carolina State University
Raleigh, NC 27695-7907

Dr. Warren Pickett
NRL Code 4692
Washington, DC 20375-5000

Prof. Max Swanson
Physics
University of North Carolina
Chapel Hill, NC 27599-3255

Dr. James Zeidler
Code 7601
NRaD
San Diego, CA 92152